Mycoplasma arginini increases activation, energetic deregulation, and tumor progression of VM-M3 metastatic macrophage cells

Author: Roberto Ettore Flores

Boston College

The Graduate School of Arts and Sciences

Department of Biology

MYCOPLASMA ARGININI INCREASES ACTIVATION, ENERGETIC DEREGULATION, AND TUMOR PROGRESSION OF VM-M3 METASTATIC MACROPHAGE CELLS.

a thesis

by

ROBERTO ETTORE FLORES

Submitted in partial fulfillment of the requirement

for the degree of

MASTER OF SCIENCE

May 2014

Abstract

TITLE: *MYCOPLASMA ARGININI* INCREASES ACTIVATION, ENERGETIC DEREGULATION, AND TUMOR PROGRESSION OF VM-M3 METASTATIC MACROPHAGE CELLS.

AUTHOR: ROBERTO ETTORE FLORES

Thesis Advisor: Thomas N. Seyfried, Ph.D.

Mycoplasmas are the smallest, self-replicating free-living prokaryotes, and have been associated with carcinogenesis. Mycoplasmas can be detected in a high percentage of a wide variety of primary human cancers. Some mycoplasma species such as *M. fermentans* and *M. hyorhinis* can transform normal murine and human cell lines into tumorigenic cells. Mycoplasma infection can activate oncogenes as well as inactivate tumor suppressor genes. These observations suggest that mycoplasmas can be both carcinogenic and or onco-modulatory. I found that the metastatic macrophage VM-M3 cell line (referred to as M3+) was infected with mycoplasmas. Mycoplasmal16S rDNA sequencing showed M3+ cells were infected by the mycoplasma species *M. arginini*. Antibiotic was used to eradicate *M. arginini* from M3+ cells (referred to as M3- cells). The energetics of the infected M3+ cells and the non-infected M3- cells was studied by measuring respiration (oxygen consumption) and fermentation (lactate production). Respiration was enhanced and fermentation was reduced in the M3- cells compared to the M3+ cells. Glucose enhanced the fermentation and reduced the respiration of both the M3+ and the M3- cells. The M3+ cells produced higher quantities of metabolites indicative of

immunological activation (itaconic acid, succinate, and citrulline) compared to M3- cells. In addition, in-vitro proliferation was higher in the M3+ cells than in the M3- cells at high cell densities. Primary subcutaneous tumor growth and metastasis was less in mice inoculated with the M3- cells than with the M3+ cells. The survival of a VM mouse was longer when inoculated with the M3- cells compared to the M3+ cells. Altogether these data indicates that *M. arginini* is an onco-modulator associated with activation, deregulated energetics and enhanced tumor progression of VM-M3 metastatic macrophage cells.

Table of Contents

List of Figures

LIST OF TABLES

LIST OF ABBREVIATIONS

AntA	Antimycin A
BMDM	Bone marrow derived macrophage cells
DMEM	Dulbecco's modified essential media
ECAR	Extracellular acidification rate
EMP	Embden-Meyerhof-Parnas Pathway
FBS	Fetal Bovine Serum
GABA	γ-Aminobutyric acid
HIF-1α	Hypoxia Inducible Factor 1-alpha
iNOS	inducible Nitric Oxide Synthase
LPS	Lipopolysaccharide (endotoxin)
MTF	Macrophage-Triggering Factor made by *M. arginini*
M3+	Spontaneous murine metastatic brain tumor cells infected with *M. arginini*
M3II+	Second clone of a spontaneous murine metastatic brain tumor cells infected with *M. arginini*
M3-	Spontaneous murine metastatic brain tumor cells not infected with *M. arginini*
M3II-	Second clone of a spontaneous murine metastatic brain tumor cells not infected with *M. arginini*
NADH	Nicotinamide adenine dinucleotide
NADPH	Nicotinamide adenine dinucleotide phosphate
NF-κB	Nuclear Factor kappa-light-chain-enhancer of activated B cells
NO	Nitric Oxide
NOS	Nitric Oxide Synthase
PPP	Pentose Phosphate Pathway
R5P	Ribose-5-Phosphate
Ru5P	Ribulose-5-Phosphate
PRPP	Phosphoribosyl Pyrophosphate
ROS	Reactive oxygen species
SDR	Presens Sensor Dish Reader
SDR	Presens Sensor Dish Reader in an airtight Coy Laboratory Chamber
TAM	Tumor Associated Macrophages
TNF-α	Tumor necrosis factor-alpha
TCA	Tri-carboxylic acid cycle
VM/Dk	Mouse strain
VM-M3 (M3)	Spontaneous murine metastatic brain tumor cells
VM-M3/Fluc	VM-M3 murine metastatic brain tumor cells expressing firefly luciferase
XF-96	Seahorse XF96 Extracellular Flux Analzyer

Introduction

Mycoplasmas of the Mollicutes class are considered the smallest self-replicating free-living prokaryotes (*1*). Mycoplasma 16S rRNA sequencing data used as a phylogenetic measure suggests that mycoplasmas originated from walled gram-positive eubacteria by degenerative evolution roughly 600 million years ago (*2*). Unlike their walled ancestors, the Mollicutes (soft skin) class lacks a cell wall and thus is resistant to common bacterial cell wall targeted antibiotics such as penicillin. Mycoplasmas range in size from 0.3μm to 0.8μm, which in turn reflects their small genome sizes. *M. genitalium* has the smallest genome (580 kb) of any organism that can be grown in pure culture and *M. hyorhinis* has the largest genome of the mycoplasmas (820 kb) (*3*) (*2*) (*4*). With limited coding capacity, the mycoplasma genus has stringent nutritional requirements for fatty acids, sterols, some amino acids, nucleic acids, and various vitamins/cofactors (*4*) (*5*). Dependence on metabolic precursors for life leads to the need of extremely complex media in order to cultivate and therefore study mycoplasmas. However, high mycoplasma infection rates show that mycoplasmas propagate well within or attached to mammalian cells in-vitro (*6*) (*1*).

Mycoplasma infection of cultured mammalian cells can falsify many metabolic and non-metabolic cellular assays including oxygen consumption assays (*7*), nitric oxide synthase activity (*8*), MTT viability assays (*9*), and mitochondrial protein synthesis determination (mycoplasma co-purified with the mitochondrial fraction) (*10*). In agreement, *M. hominis* infection of HeLa cells significantly altered genetic expression

profiles of 1972 genes (*11*). Another study found approximately 200 significant expression profile alterations in infected MCF7 cells and 70 of those genes were involved in metabolism (*12*). In Mycoplasma pneumoniae-infected individuals, tracheal cell explants were shown to have a decrease in ATP from respiration, possibly due to lower dehydrogenase activities of the cells (*10*). Similarly, M. hyorhinis is also capable of reducing the respiration system in heavily contaminated human skin fibroblast cells (*13*). Thus, mycoplasmas have a high potential for modulating host metabolism.

Regarding energy catabolism, mycoplasmas can be classified as fermentative or non-fermentative (*14*). Fermentative mycoplasmas are able to gain energy by substrate-level phosphorylation of ADP by glycolysis, specifically by the Embden-Meyerhof-Parnas (EMP) Pathway (*14*). Fermentation produces acid and occurs not to specifically make energy, but rather to oxidize NADH to allow glycolysis to continue to make energy (NAD+ is required for the 6^{th} step of glycolysis) (*15*). Therefore, fermentative mycoplasmas are acidifiers and thus reducers of their environment. Some fermentative mycoplasmas such as *M. gallisepticum* have the ability to carry out a non-fermentative catabolism (*16*) (*17*) but viability and growth during a non-fermentative catabolism are unclear. However in the presence of glucose, fermentative mycoplasmas produce ***a net waste of acid***. In contrast, non-fermentative mycoplasmas do not produce a net waste of acid or alcohol, which indicates that their energy catabolism is mainly oxidative. In part, the oxidative catabolism of the non-fermentative mycoplasmas is perhaps due to the lack of

phosphofructokinase and aldolase activity of the EMP pathway in these organisms (*14*). Thus, respiration (oxidation) rather than fermentation (reduction) characterizes the non-fermentative mycoplasmas.

Even though non-fermentative species of mycoplasma seem unable to ferment glucose, they possibly generate energy anaerobically through the arginine dihydrolase pathway (*18*). However, the aerobic or anaerobic contribution of the arginine dihydrolase pathway to overall energy generation in any one species is unclear. Some non-fermentative mycoplasma species require arginine for growth, while other species can grow without arginine. For example, only one of three strains of *M. arginini* was found to require arginine for growth (*19*). *M. arginini* was named as so simply because the author discovered that arginine boosted growth, rather than glucose or urea. (*20*). Whether arginine is utilized by non-fermentative mycoplasmas more for catabolic or anabolic needs is unclear (*21*) (*19*) (*22*). Since *M. arginini* contains a flavin-terminated respiratory chain it is likely that *M. arginini* uses both respiration and the arginine dihydrolase pathway for energy production according to oxygen levels and metabolic fuel supply set by the environment (*19*). In hypoxic conditions that may not allow for sufficient energy generation from respiration, arginine-utlizing mycoplasma would most likely generate energy through the anaerobic arginine dihydrolase system, just as the fermentative mycoplasmas would generate energy through anaerobic lactate fermentation.

Even though the interaction between host and mycoplasma is typically commensal,

mycoplasmas are well known for their parasitic nature (*23*), partly due to their fastidious metabolic needs (*4*) and partly due to their ability to promote chronic inflammation (*24*). Various strains of mycoplasmas are capable of causing disease as well as implicated as co-factors in dozens of others, but their virulent capabilities and potential are just beginning to unfold (*25*) (*26*) (*27*) (*23*) (*24*). Irrespective of the role mycoplasmas play in disease as benign colonist, co-contributors, or even the cause, they have a robust ability to modulate inflammation, metabolism, and cancer.

A search for the link between mycoplasmas and cancer began after some mycoplasma species were shown to be sufficient in causing non-tumorigenic cells to transform into tumorigenic cells (*28*) (*29*). In addition to the classic hallmarks of cancer, an emerging hallmark is deregulated energetics (*30*). As detailed above, mycoplasmas seem sufficient in deregulating cellular energetics. Also, mycoplasmas have been shown to induce cells to evade apoptosis (*31*) (*32*), sustain proliferation (*24*) (*5*), enable replicative immortality (*33*), and activate invasion and metastasis (*34*) (*35*), which are all four classic hallmarks of cancer (*30*). Alongside the deregulating of cellular energetics, the other emerging hallmark of cancer cells is the ability to avoid immune destruction. Recently, mycoplasma infected tumor cells were found to release exosomes that activate inhibitory B-cells, which in turn inhibit T cells cytotoxic to cancer cells (*36*). Interestingly, mycoplasmas also cause genomic instability (*37*) (*38*) and **inflammation** (*39*) (*40*), both major **hallmark-enabling characteristics** of neoplasia. In addition, mycoplasma infection is strongly

associated with onco-genetic alterations. During transformation of non-tumorigenic C3H mouse embryo cells into tumorigenic cells, *M. fermentans* and *M. penetrans* have been shown to cause constitutive H-ras and c-myc expression (*41*). Moreover, *M. arginini* infection has been shown to cooperate with oncogenic Ras, activate NF-kB, and suppress p53 (*32*). All mycoplasma species tested by these authors suppressed p53, but *M. arginini* showed the greatest ability to suppress p53. In addition to mycoplasma infection being strongly linked to the hallmarks and characteristics of cancer, their presence in a variety of human primary tumor samples strengthens the possibility of a causative or at least a modulatory role in human carcinogenesis (*28*) (*42*) (*43*) (*44*) (*45*). The ability of mycoplasmas to cause chronic inflammation and activate NF-kB further strengthens the link between mycoplasma, inflammation and cancer.

Although some immune cells can help eradicate tumor cells, inflammation created by tumor-associated immune cells ultimately balances out towards that of tumor promotion rather than of regression (*46*). In agreement with the surprising and counterintuitive findings that immune cells ultimately promote tumor progression, tumor-associated immune cells have been found to enable some of the hallmarks of cancer (*30*). Many types of immune cells are able to promote tumor progression, including T lymphocytes, B lymphocytes, and macrophage subtypes (*47*) (*48*). Typically, type M2 macrophages are thought to stimulate cancer progression while type M1 macrophages have been shown to be important for tumor regression (*48*). However, Egeblad et al. suggest that tumor-associated macrophages (TAM) may be a

continuum of various M1 and M2 subtypes rather than rigidly being classified as solely M1 or M2 (*49*). Regardless of the exact type of macrophage, the transcription factor Hypoxia Inducible Factor 1-alpha (HIF-1α) has been described to be a master regulator for tumor promoting TAM (*50*). The HIF-1α expression of TAM links tumor-promoting inflammation and deregulated cellular energetics, i.e. a hallmark-enabling characteristic of cancer with an emerging hallmark of cancer, respectively (*51*). Tumor-promoting inflammation is referred to as "smoldering" because of its chronic and low-grade nature (*52*). Interestingly, mycoplasma-induced inflammation seems to recapitulate tumor-promoting inflammation as both are NF-κB-driven, chronic and low-grade in nature (*53*). The link between infection, chronic inflammation, and cancer has been noted (*54*).

My study investigates the metabolic and tumorigenic consequences of *M. arginini* infection in metastatic murine macrophage tumor cells (VM-M3 cells). The VM-M3 tumor arose spontaneously in the cerebrum of a male adult VM/Dk mouse. The VM-M3 cells (M3) are more specifically characterized as microglia since they express morphological, behavior, biochemical, and genetic properties of macrophages (*55*). When inoculated in the syngeneic VM mouse host, M3 cells recapitulate all major biological processes of metastasis to include local invasion, intravasation, immune system survival, extravasation and secondary tumor formation involving liver, kidney, spleen, lung and brain (*55*). Inoculation of M3 directly into the brain seems to biologically mimic the characteristics of glioblastoma seen in the human (*56*). In the present study the M3 cells were diagnosed with an *M. arginini* infection,

however the origin or date of the infection is unclear. After eradication of *M. arginini* from M3 cells, the energy catabolism and other metabolic pathways between the infected (M3+) and non-infected (M3-) cells were assessed. In addition, the differential effects of the M3+ and M3- cells inoculated in-vivo were examined. My data suggests that *M. arginini* is capable of increasing tumor progression possibly through tumor-promoting inflammation and deregulation of cellular energetics. Since mycoplasmas can be detected in a high percentage of a wide variety of primary human cancers (*28*) (*42*) (*43*) (*44*) (*45*), therapies targeting mycoplasma-infected tumors may benefit cancer patient survival.

Materials and Methods

Cell lines and culture conditions

The VM-M3+ cell line was established from flank-grown VM cerebral tumors as previously described (*55*). VM-M3 (M3) cells were grown in Dulbecco's modified Eagle medium (DMEM, Sigma, St. Louis, MO) with high glucose (25 mM) supplemented with 10% fetal bovine serum (FBS, Sigma) and 50 lg/ml penicillin–streptomycin (Sigma). M3 cells were cultured in a CO2 incubator with a humidified atmosphere containing 95% air and 5% CO2 at 37C. The M3 cells were passaged approximately one time per week or when 80% confluency was reached. The M3II cells (clone II) were treated exactly as the M3 cells.

Eradication and Identification of Mycoplasma

VM-M3 cells were eradicated by adding MycoZap (Lonza) to the culture media for one week, with the starting point being right after cells plated down to the culture plastic at low density (100,000 cells/100mm dish). In a separate incubator a control dish of VM-M3 cells with no mycoplasmal targeted antibiotics was treated and passaged in conjunction with the MycoZap treated dish at all times. The media was changed every 48 hours and no change in growth or cell death was noted. A subsequent treatment of ciprofloxacin (10ug/mL) was used for one week as a prophylactic strategy exactly as described for MycoZap above. After one week of ciprofloxacin prophylactic treatment the VM-M3 cells were grown for an additional week only with the usual Penicillin/streptomycin antibiotics, which were not

removed during MycoZap/Ciprofloxacin treatments. Treated VM-M3 cells and untreated VM-M3 cells were subjected to a MycoAlert Detection Assay and e-myco Plus PCR detection (Bulldog Bio)(Figure 1) to verify eradication of infection. Identification of *M. arginini* infection was done by excision and sequencing of the positive 260 bp 16S rDNA band in an e -Myco plus Mycoplasma PCR Detection Kit 1.5% agarose gel. The mycoplasmal 16S rDNA sequence (query) was BLAST searched against the GenBank database and the best match (subject) or top score was *Mycoplasma arginini*.

Oxygen consumption and Extracellular Acification Rate, and Lactate Measurements

Oxygen consumption rate and Extracellular acidification rate (ECAR) was taken with a Seahorse XF96 Extracellular Flux Analzyer. M3+ or M3- cells were seeded at 30,000 cells per XF96 plate well and allowed to incubate for 12 hours in DMEM high glucose with 10% FBS. The media was then changed to complete media with or without 100 nM Antimycin A (complete media: DMEM with 2 mM glutamine, 10mM glucose, and 0.5 mg/mL Albumax I. No FBS and no bicarbonate were included in the media as recommended by Seahorse for ECAR measurements. Phenol red was not included since visual pH monitoring was unnecessary. The Crabtree effect was circumvented by simply not including glucose in complete media). Two hours later the media was changed again to complete media and the plate was quickly inserted into the XF96 analyzer. The XF96 analyzer was programmed to take 7 minute measurements with a 1-minute mix and a 1-minute wait period before a subsequent

7 minutes measurement was taken. The total measurement time was 2 hours and the average O2 consumption was calculated. O2 consumption rate and ECAR were steady throughout the 2 hour time period.

Lactate production rate was assessed by collection of the media of each XF analyzer 96-well with a subsequent Eton Bioscience's L-lactate assay I kit. Taking the millimoles of lactate and multiplying by the total microliters in each well determined the total millimoles of lactate. The total O2 consumption rate, ECAR value, and lactate production rate was corrected to the milligram protein in each XF96-plate well. Thus, oxygen consumption, ECAR, enzymatic lactate, and protein were all measured from the same well.

To assess oxygen consumption in the M3II clone a Presens Sensor Dish Reader (SDR) in an airtight Coy Laboratory Chamber was utilized (termed the SDR plus). The percentage of gas in the chamber was set at 20% oxygen, 5% CO2, and 75% N2. 125,000 cells/ml were seeded in a 24-well PreSens OxoDish® plates in 500 ul of DMEM high glucose plus 10% FBS and allowed to settle for 3 hours before addition of new DMEM high glucose 10% FBS at which t=0. Cell # was assessed with a Millipore Scepter. The cell number per well was the same for BV-2, M3LM and M3 at time of initial seeding. While the cells incubated the SDR Plus assessed % O2 at the bottom of the dish every 3 minutes for 48 hours. Since there is 20% O2 in the SDR plus environment (translating to > 20 % in the media), the % O2 recorded in wells

with cells is subtracted from no cell containing wells to yield the %O2 consumed at 48 hours.

Western Blot

For western blot analysis, VM-M3+ and VM-M3– cells were lysed in ice-cold RIPA lysis buffer containing 1x TBS, 1% Nonidet P-40, 0.5% sodium deoxycholate, 0.1% SDS, and 0.004% sodium azide supplemented with PMSF, protease inhibitor cocktail, and sodium orthovandate (Santa Cruz Biotechnology, Inc., Santa Cruz, CA, USA). Lysis was performed on ice for 30 minutes. Protein was then obtained by centrifugation at 12,000 x g for 20 minutes at 4°C. The amount of protein in the sample was determined using the Pierce BCA Protein Assay (Thermo Scientific). Samples containing 20 μg of protein were boiled in NuPAGE LDS Sample Buffer and separated on NuPAGE 4%–12% bis-Tris gels (Invitrogen). The proteins were electrophoretically transferred to a Low-Flourescence PVDF Transfer Membrane at 20 V overnight at 4°C. The membrane was blocked in Odyssey Blocking Buffer for 1 hour and then probed with antibodies against Complex IV, subunit IV (1:2,000) (clone 20E8; Molecular Probes, Eugene, Oregon, USA), LDHA (1:1,000) (#2012S; Cell Signaling Technology, Danvers, MA, USA), and β-actin (1:7,500) (Clone AC-74; Sigma-Aldrich) overnight at 4°C. The blots were then incubated with the corresponding Odyssey secondary antibodies Goat anti-Rabbit IRDye 800CW (1:20,000) (827-08365) and Donkey anti-Mouse IRDye 800CW (1:20,000) (926-32212) (LI-COR Biosciences). The proteins were visualized using the Odyssey Classic imaging system (LI-COR Biosciences). The intensity of each band was

determined using Image Studio Lite software (LI-COR Biosciences). Complex IV, subunit IV and LDHA expression were normalized to the intensity of the β-actin band. Statistical analysis was performed using IBM SPSS Statistics software. A two-tailed t-test was performed and the significance values were determined for the ratios of both Complex IV, subunit IV and LDHA to β-actin for both VM-M3 + and VM-M3 – cells.

Protein Quantification

For protein determination of Seahorse XF96 assay plates, 40 μl of RIPA lysis buffer (described above in detail for Western Blot) was added to each aspirated well and mixed by pipetting up and down 25 times. The plates were then incubated on an orbital shaker for 15 minutes at 200 rpms. The mixing step was repeated, the plate was incubated on ice, and the protein was subsequently quantified using 25 μl in the Pierce BCA Protein Assay (ThermoScientific) according to the manufacture's protocol. Protein quantification for proliferation assays was done in the same manner.

Proliferation and Luminescence Output Assays

ATP determination over 2 days in black walled 96-well cell culture treated plates was used to assess in-vitro proliferation of M3+ and M3— cells initially seeded at 15,000 cells/well. The cooled CCD camera on the Xenogen IVIS Lumina system (Xenogen, Hopkington, MA) was used to record the photons / second (over 10 seconds) emitting from a luminescence reaction after performing a CellTiter-GLO

Luminescent ATP assay (Promega, Madison, Wisconsin) according to the manufacture's protocol. In addition, in-vitro proliferation over 5 days of M3+ and M3- cells seeded at 5,000 cell/well in 96-well cell culture plates was assessed using a Pierce BCA protein assay. At 1, 3, and 5 days the protein was collected from each well as described in Protein Quantification section above. For the luminescent output assay the same procedure as the ATP proliferation assay was used, however with the following changes: rather than the CellTiter-GLO assay, the M3 cell endogenous firefly luciferase vector and added D-luciferin (Promega) was used to initiate the bio-luminescence reaction. Also, cells were not allowed to proliferate as the bio-luminescence was gauged at 4 hours after seeding M3+ or M3- cells (M3 cells attach to the bottom of the dish in ~ 2 hours). During the luminescence output assay progressive microgram amounts of luciferin were added to a 120ul of growth media with 30,000 cells / well in a black walled 96-well cell culture treated plate.

Mice

Mice of the VM/Dk (VM) strain were obtained as gifts from G. Carlson (McLaughlin Research Institute, Great Falls, Montana) and from H. Fraser (University of Edinburgh, Scotland). All VM mice used in this study were housed and bred in the Boston College Animal Care Facility using husbandry conditions as described previously (*57*). All animal procedures were in strict accordance with the NIH Guide for the Care and Use of Laboratory Animals and were approved by the Institutional Animal Care Committee.

Subcutaneous inoculation of M3+ and M3- cells

The M3+ and M3- cell lines were grown to confluency in 245 mm cell culture dishes, scraped in PBS containing 25 mM glucose and 4 mM glutamine (PBS+), washed and then re-suspended in PBS+. Subsequently, 1.5 million M3+ or M3- cells were subcutaneously injected in a 0.5 mL volume of PBS into the back or flank region of VM/Dk mice.

Assessment of tumor progression in VM mice

Morbidity of VM/Dk mice was used as an endpoint to in-vivo experiments I, II, and the metastasis/survival study using M3II clones. However, in experiments I and II M3- inoculated mice were not morbid but were sacrificed in order to compare tumor progression to M3+ inoculated mice. For experiments I and II, primary tumors were excised, frozen, and weighed. In the metastasis/survival study using M3II clones, mice were imaged with the Xenogen IVIS Lumina system (Xenogen, Hopkington, MA) to record the bioluminescent photon signal from the VM-M3/Fluc tumors. For in vivo whole body imaging in the metastasis / survival study, mice received an i.p. injection of D-luciferin (50 mg/kg, Xenogen) and Avertin (0.1 ml/10 g) and mice were imaged for 1 minute. For ex vivo imaging during in-vivo experiment II, the brain was excised and placed in a Petri dish with 300 mg/ml D-luciferin in PBS, and imaged for 10 seconds.

Extraction of Metabolites and Capillary Electrophoresis Time-of-Flight Mass Spectrometry

M3+ and M3- cells were incubated in complete media (DMEM amino acid mixture, 10 mM glucose, 2 mM glutamine, and Invitrogen's albumax I; no bicarbonate, phenol red, or FBS added) for 6 hours in an incubator with 100% air at 37C (0% CO2). Subsequently after washing the cells twice in a 5% (w/v) mannitol water solution the metabolites were extracted with methanol and an internal standard water solution. The samples were kept on ice, ultra-filtered in custom Human Metabolome Technology centrifugal tubes at 4°C, and the flow through was vacuum dried for ~ 2 hours. Metabolome analysis was performed by HMT using Capillary Electrophoresis Time-of-Flight Mass Spectrometry in two modes for cationic and anionic metabolites. The analysis detected 173 metabolites (89 metabolites in cation mode and 84 metabolites in anion mode) on the basis of HMT's standard library.

Results

Discovery and Eradication of Mycoplasma Infection in VM-M3 cells

Mycoplasma infection in VM-M3 cells was first diagnosed enzymatically with a MycoAlert® Mycoplasma Detection Kit (data not shown). In light of a positive infection, the VM-M3 cells are referred to as VM-M3+ (abbreviated M3+). To verify the enzymatic detection of mycoplasma, PCR amplification of a 260 bp region of mycoplasmal 16S rDNA gene was performed using primers able to identify 182 species of mycoplasma. Positive amplification indicative of a positive infection was seen by the presence of a 260 bp band in the +control and M3+ lane (Figure 1A). After eradication of mycoplasma infection with mycoplasma-targeted antibiotics, no band at 260 bp could be detected indicating a successful eradication (M3- lane). After eradication and in light of a negative infection, this cell line was named M3-. Three weeks after eradication, the M3- cells remained free of mycoplasma infection (Figure 1B).

Mycoplasma arginini infection of VM-M3 cells

The 260 bp region of amplified mycoplasmal 16S rDNA gene from the infected M3+ cells was excised from the gel, purified, and sequenced. BLAST was used to align the mycoplasmal 16S rDNA (query) to subject sequences in GenBank. The top score identified the query sequence as derived from *Mycoplasma arginini* (Figure 2A). The 16S sequence belonging to *Mycoplasma hominis*, a phylogenetically close

relative to *M. arginini*, (*2*) received a lower score in light of the mismatch/gap alterations (Figure 2B).

Influence of *M. arginini* on respiration in VM-M3 cells

According to bioenergetics principles mammalian cells are able to respire amino acids and fatty acids for energy (*15*) (Figure 3). In order to compare the respiratory systems in M3+ and M3- cells, a Seahorse XF96 analyzer was utilized (Figure 4). In the presence of amino acids, fatty acids, and glucose (complete media) the eradicated M3- cells show an elevated respiration rate compared to the infected M3+ cells (Figure 5A). Oxygen consumption rate dropped by 84% and 85% in M3+ and M3- cells, respectively, following addition of the respiratory inhibitor Antimycin A (AntA). Thus, approximately 15% of oxygen consumption in both cell lines is unassociated with respiration in complete media. *M. arginini* eradication in M3- cells elevated respiration by 29%, after subtracting the AntA insensitive oxygen consumption.

Extracellular acidification rate (ECAR) is often used to estimate lactate fermentation. However, ECAR is an indirect measure of lactate fermentation as the protons expelled with lactate are measured rather than lactate. ECAR is higher in the M3- cells than in the M3+ cells and fails to elevate under AntA treatment in M3+ cells (Figure 5B). Direct enzymatic measurement of L-lactate is preferred as a more reliable measure of lactate fermentation rate as many factors can influence pH other than lactate efflux.

As an alternative to ECAR, an enzymatic assay was used to estimate lactate production (a measure of fermentation). Unlike the ECAR value, lactate production increased in M3+ when respiration was inhibited by AntA, as would be expected (Figure 5C). Lactate production was greater in M3- cells than in M3+ cells in the presence of AntA. No difference in lactate production was found between M3+ and M3- when lactate production was corrected to protein levels (Figure 5C). However, when lactate production was corrected to ATP levels and cell number, M3- cells made less lactate than M3+ cells (Figure 6). When compared to the M3+ cells, the reduced lactate production by M3- cells is in agreement with their higher respiration rate. The lower respiration and higher fermentation of M3- cells compared to M3+ cells is unable to be explained by differences in Cytochrome C Oxidase and LDHA protein levels (Figures 7A-&D)

Influence of *M. arginini* on the Crabtree effect in VM-M3 cells

Cancer cells and other non-tumorigenic highly glycolytic cells experience a Crabtree effect, i.e. glucose-induced suppression of respiration (*58*) (*59*) (*60*). Suppression in respiration from a Crabtree effect can be measured by using media devoid of glucose, since respiration becomes un-suppressed (*61*). Both the M3+ and the M3- cells demonstrated a Crabtree effect when 10 mM glucose (+glc) was added to glucose-absent media (-glc) that consisted an amino acid mix, 2 mM glutamine, and albumin conjugated fatty acids (Figure 8A). The M3+ and M3- cells experienced a 21% and 30% Crabtree effect, respectively, when solving for the % Crabtree effect

equation of Wenner (*59*) (Table 1 & Figure 8B). In other words, glucose addition suppressed the respiration of M3+ and M3- cells by 21% and 30%, respectively.

Respiration rate measured during the Crabtree is misleading because of variability in % Crabtree effect of difference cell lines. Unsuppressed-respiration (during Crabtree effect-circumvention) is a more accurate indication of a cell lines maximum respiratory rate. During the Crabtree effect the M3- cells have a 29% increase in respiration compared to M3+ cells. However, when the Crabtree effect is circumvented by glucose removal the M3- cells show a 37% increase in respiration over that of M3+ cells (Figure 8A). Regardless of the presence or absence of the Crabtree effect, *M. arginini* eradication results in a significant increase in respiration rate in VM-M3 cells.

Influence of *M. arginini* on activation metabolites in VM-M3 cells

Several activation-specific metabolic markers for macrophages are characterized and validated. Itaconic acid is a bactericidal product of activated macrophages (*62*) (*63*) (*64*). The production of itaconic acid dropped more than two-fold in the M3- cells compared to the M3+ cells (Figure 9). Another key metabolite recently found to be produced by activated macrophages is succinate, which is metabolized partly from GABA (the GABA shunt) (*65*). GABA and succinate was significantly reduced in M3- cells compared to M3+ cells (Figure 10). In addition to itaconic acid and succinate, another indicator of macrophage activation is Nitric Oxide (NO) made by Nitric Oxide Synthase (NOS) by metabolism of arginine to citrulline (*66*)(*67*).

Therefore, arginine metabolism to citrulline indicates NO production. In the infected M3+ cells arginine metabolism to citrulline was detected compared to barely detectible arginine to citrulline metabolism in the M3- cells (Figure 11).

Influence of *M. arginini* on the in vitro proliferation of VM-M3 cells

Elevated intra-cellular metabolites of the Pentose Phosphate Pathway (PPP) metabolites are indicative of enhanced cellular proliferation, as the PPP supplies metabolic precursors for DNA and RNA synthesis (*68*). Glucose is the precursor for the synthesis of Ribose-5-Phosphate (R5P), Ribulose-5-Phosphate (Ru5P), and Phosphoribosyl Pyrophosphate (PRPP). R5P, Ru5P, and PRPP provide the necessary ribose for de novo nucleic acid synthesis (*69*). The M3+ cells showed elevated intra-cellular levels of the PPP metabolites R5P, Ru5P, and PRPP compared to the M3- cells (Figure 12). Reduced intra-cellular PPP metabolite concentration was concomitant with a reduced proliferation rate at higher cell densities in the M3- cells compared to the M3+ cells (Figure 13). Therefore, eradication of *M. arginini* resulted in a lower in-vitro proliferation rate in M3 cells only at high cell densities.

Influence of *M. arginini* on the in vivo tumor growth of VM-M3 cells

The M3+ cells metastasize systemically following subcutaneous inoculation in the syngeneic VM/Dk mouse host. Approximately 1.5 million M3+ or M3- cells were inoculated subcutaneously in the back (experiment 1) or the flank (experiment 2) of the VM/Dk mice. Experiment 1 was terminated after 21 days and experiment 2 was terminated after 30 days when the mice with the M3+ cells became moribund

(reduced ambulation due to tumor burden). None of the mice inoculated with M3- cells became moribund. Wet weight was less for the tumors produced from the M3- cells than for the M3+ cells (Figure 14A & 14B).

Influence of *M. arginini* on the *in vivo metastasis of* VM-M3 cells

The M3+ cells are tranduced with a firefly luciferase lentivirus vector under the control of the constitutive CMV promoter. By injecting luciferin into VM mice it is possible to monitor growth and movement of M3 cells in-vivo by detecting the emitting photons (Figure 15). Oxygen is a necessary substrate for the luciferase light-emission reaction. The M3+ cells consumed less oxygen than the M3- cells (Figures 5 and 8A). In addition, the M3+ cells produce less light than M3- cells from the luciferase reaction (Figure 16).

In experiment 2, metastasis to liver and brain was assessed. Metastatic nodules to liver and metastatic brain luminescence were qualitatively less in M3- inoculated mice compared to M3+ mice (Figure 17). Brain luminescence in M3- mice was reduced by a factor of 2.66 to account for the greater luminescence output of the M3- cells compared to the M3+ cells.

Influence of *M. arginini* on oxygen consumption and tumor progression in a VM-M3 tumor variant clone

Cells comprising tumors are genetically heterogeneous and therefore it is possible that two clonal cell lines created from the same tumor can exhibit different metabolotypes. In order to control for this phenomenon, a different clone of the VM-M3 tumor (M3 clone II) was isolated from a firefly luciferase transduced-monolayer of cells from a separately passaged VM-M3 tumor chunk that gave rise to the M3 cells (original clone). M3 clone II (M3II) also tested positive for mycoplasma infection (M3II+) via the enzymatic mycoalert (Lonza) assay and was eradicated (M3II-) with a 1 week treatment of MycoZap (Lonza). Using an SDR plus system to measure oxygen consumption, eradicated M3II- cells showed a marked elevation of respiration compared to the M3II+ cells (Figure 18A). When M3II+ and M3II- cells were inoculated in VM mice (1 mouse for each cell line) the eradicated M3II- cells showed reduced primary tumor growth, metastasis, and longer survival (Figure 18B). These results with a different clone of the VM-M3 tumor (M3II) are in agreement with studies done with the original clone (M3).

Discussion

M. arginini-infected M3 cells produce metabolites suggestive of activation.

M. arginini produces a low molecular weight protein termed Macrophage-Triggering Factor (MTF) that activates macrophages (*70*). Once activated, macrophages and microglia exert cytotoxic effects by releasing inflammatory mediators, such as arachidonic acid metabolites, interleukin-1 (IL-1), nitric oxide (NO), reactive oxygen species (ROS), and tumor necrosis factor-alpha (TNF-α) (*71*) (*72*). In fact, macrophages are potent secretory cells that release a plethora of mediators in response to activation (*73*). One of these activation markers was recently shown to be itaconic acid (*62*), which was corroborated in a subsequent independent study (*63*). Itaconic acid is a small metabolite that inhibits bacterial isocitrate lyase as well as glycolysis via the inhibition of phosphofructokinase (*64*) (*74*) (*75*). Therefore, itaconic acid could be both a bactericidal and an anti-glycolytic metabolite. The M3+ cells produce more than two-fold the amount of itaconic acid than M3- cells suggesting that M3+ cells have an elevated levels of activation compared to the M3- cells (Figure 8).

Another metabolite made by activated macrophage cells is succinate (*65*). In activated bone marrow derived macrophage cells (BMDM) succinate is made partly through the GABA shunt, which shunts GABA metabolized from glutamate towards succinate production. The LPS-induced succinate production of BMDM results in HIF-1α stabilization, elevated glycolysis, and subsequent IL-1β production. In

addition, BMDM activation results in a down-regulation of mitochondrial genes and up-regulation of glycolytic genes suggesting that activation of BMDM leads to lower respiration and a higher fermentation. In agreement, a separate study documented that LPS/IFN-γ -activated macrophages also experience a shift from respiration to fermentation, however succinate efflux was not measured (*66*). In the present study, M3+ macrophage cells showed elevated succinate efflux (Figure 9) in addition to the previously discussed diminishment in respiration (Figures 5A and 8A). Altogether, the present study and previous studies (*65*) (*66*) indicate that activated macrophage cells experience a diminished respiration as well as an elevated succinate efflux. Therefore, elevated succinate efflux is either a direct response to macrophage activation or a direct response to a diminished respiration. Tumor cells with a TCA cycle respiratory defects also elevate succinate efflux (*76*). Further, succinate levels elevate in oxygen deprived diving animals, oxygen-deprived rabbit heart, and oxygen-deprived tumor cells (*77*) (*78*) (*79*). Thus, elevated succinate seems to be more of a response to a diminished respiration than to the activated state of macrophages. A likely scenario is that macrophage activation in-vitro leads to a diminished respiration and a diminished respiration leads to elevated succinate efflux. Therefore, succinic acid is emerging as a candidate metabolic marker for a diminished respiration and a diminished respiration seems to be a response of activated macrophages in-vitro.

Arginine is also an important metabolite in macrophage cells, *M. arginini* metabolism, and the cancerous state (*19*) (*80*) (*81*) (*82*). In the present study,

metabolomic analysis showed an arginine to citrulline metabolism in the M3+ cells. Arginine to citrulline metabolism indicates the production of Nitric Oxide (NO). NO is a sign of macrophage activation and is made by inducible Nitric Oxide Synthase (iNOS), an enzyme that metabolizes O2, NADPH and arginine to water, citrulline and NO. Since NO is difficult to measure and because no other enzyme is known to metabolize arginine to citrulline in mammalian cells, NOS activity and NO can be conveniently assessed by measuring conversion of radio-labeled arginine to citrulline (*67*). I speculate that the M3+ cells are producing NO on the basis of a drop in arginine levels compared to the M3- cells coupled with citrulline production, which is absent in the M3- cells (Figure 10). On the other hand the arginine to citrulline metabolism in the M3+ cells may stem from the metabolism of *M. arginini* itself. Arginine deiminase from arginine-utilizing mycoplasma like *M. arginini* also metabolizes arginine to citrulline. As a result arginine deiminase has been found to be masquerading as nitric oxide synthase in mycoplasma infected cultures (*8*). Thus it is unclear whether the arginine to citrulline metabolism measured in M3+ cells indicates activation-induced NO production or whether it is simply a product *M. arginini* arginine deiminase metabolism. Activation-induced NO production is the more likely scenario explaining arginine to citrulline metabolism since M3+ cells also showed elevation of activation-associated itaconic acid and succinate production. In agreement with the concept that arginine to citrulline metabolism results in NO production in M3+ cells, the presence of *M. arginini* is sufficient to cause NO and TNF-α production in macrophage cells (*70*) (*83*).

Elevated proliferation associated with *M. arginini* infection is dependent on high cellular density

The enhanced proliferation in M3+ cells is concomitant with an increase in the macrophage activation-metabolites itaconic acid, succinate acid, and citrulline. However, M3+ cells show no increase in proliferation in low-density culture suggesting that M3+ cells may not be activated at low cellular density. Therefore, *M. arginini* only exerted its mitogenic effects at high cellular density. The increased proliferation of M3+ cells over M3- cells at high cell density could be a result of an activation product that concentrates in the culture media. For example, mycoplasmas have been shown to induce macrophages to secrete granulocyte-monocyte colony stimulating factors (GM-CSFs) (*5*), which may accrue in the cell culture media to cause proliferation during high-density M3+ cell culture. Further studies with the M3+ cells in low and high density will be needed to uncover the mechanism behind the increase of high-density proliferation of the M3+ cells over that of the M3- cells.

Crabtree effect-induced suppressed respiration is separate from *M. arginini*-induced diminished respiration

All cancer cells are known to experience a Crabtree effect and there is no mention in the literature of cancer cells that fail to do so (*84*) (*85*) (*86*). Normal non-transformed, non-tumorigenic cells do not experience a Crabtree effect (*58*) (*59*). Some activated immune cells experience a Crabtree effect (*60*), but it is unclear

whether these Crabtree positive immune cells would persist to experience a Crabtree effect in the non-activated state. The Crabtree effect seems to be derived from a over-sensitive hyperactive glycolytic system that siphons the ADP pool away from respiration and thus suppresses respiration (*59*) (*87*), however it is unknown how this deregulation of glycolysis is initiated. Therefore the lactate produced during the Crabtree effect is not due to an increased glycolysis but rather from the suppressed respiration system. Since glucose is always present in-vivo and in-vitro, cancer cells experience a constant diminished respiration due to the suppressive effects of the Crabtree effect. In agreement, our study shows that both tumorigenic M3+ cells and M3- cells experience a Crabtree effect (Figure 8A). It is unclear why M3+ cells have a smaller % Crabtree effect than the M3- cells (Table 1), however a reduced Crabtree effect like seen in the M3+ cells has been associated with uncoupling of respiration with phosphorylation of ADP (*59*). Thus in concordance with their tumorigenicity and as a result of the ubiquitous nature of glucose, both *M. arginini*-infected M3+ cells and eradicated M3- cells experience a glucose-induced constitutive diminished respiration due to the Crabtree effect.

In addition to the diminished respiration caused by the Crabtree effect, the infected M3+ cells experience another separate reduction in respiration compared to the M3- cells (Figure 5A & 7). Presumably the separate reduction in respiration is due to the presence of *M. arginini.* The *M. arginini*-associated reduction in respiration of the M3+ cells is separate from the reduction caused by the Crabtree effect. As a result the *M. arginini*-associated reduction in respiration is seen in the Crabtree

positive condition (+glucose) and also when the Crabtree effect is circumvented (-glucose). When the Crabtree effect is circumvented in both M3+ and M3- cells, the *M. arginini*-associated reduction in respiration is exacerbated (Figure 7: Compare M3+ and M3- minus glucose condition). Thus, the M3+ cells exhibit two insults to respiration, one being the Crabtree effect and the other being the "*M. arginini* effect" per se.

Diminished respiration is concomitant with enhanced fermentation in VM-M3 cells infected with *M. arginini*

Respiration and fermentation negatively regulate each other and therefore are intrinsically linked. For example, during the Crabtree effect glucose induces an over-active fermentation and as a result the respiration system is suppressed (*59*). In agreement, hypoxia and respiratory inhibitors halt respiration and fermentation is up-regulated to energetically compensate for lost respiration. However, the reduced respiration of M3+ cells compared to M3- cells is not accompanied by an increase in fermentation after correction of the fermentation rate (lactate production) to the milligrams of protein (Figure 5C). Similarly, the M3+ cells would be expected to increase lactate fermentation rate to the same extent as the M3- cells when challenged with the respiratory inhibitor Antimycin A, but M3+ cells produce significantly less lactate than the M3- cells (Figure 5C + Ant A condition). The possibility exists that *M.arginini* is respiring the lactate produced by M3+ cells and thus an increase in fermentation rate would be masked. Respirometry studies have shown that both fermentative and non-fermentative mycoplasmas can respire

lactate and various other metabolic fuels for energy. *M. hominis*, a non-fermentative mycoplasma similar to *M. arginini* , is able to respire butyryl-CoA, succinate, NADH, NADPH and lactate (*88*) (*89*). The fermentative *M. gallisepticum* can also respire lactate and various other mycoplasma species have been shown to respire ethanol, glucose, acetate, and short chain fatty acids (*90*). Therefore, *M. arginini* could possibly be respiring the lactate produced by M3+ giving the false impression that fermentation rate is not increasing. The possibility that *M. arginini* is interfering with lactate measurements in the this study is in agreement with previous reports on mycoplasma falsifying many metabolic and non-metabolic cellular assays (*8*) (*9*) (*10*).

Another more substantiated reason that *M. arginini* could be interfering with lactate measurements is the fact that lactate production was corrected to the milligram protein and that the protein content of M3+ cells could be overestimated due to the addition of *M. arginine*-derived protein. For example, if *M. arginini* protein amounted to 10% of the total *M3+* protein quantified then the actual M3+ protein would be incorrectly overestimated. An overestimation of M3+ protein results in an underestimation of the fermentation rate (nmoles lactate / hr / mg protein value used in Figure 5C). In support of this notion, the extracellular lactate concentration measured by mass spectrometry was greater for M3+ cells compared to M3- cells since the mass spectrometry data was corrected to cell number rather than to milligram protein (Figure 18A). Additional evidence that M3+ cells increase fermentation in response to diminished respiration is derived from studies done

with M3II cells, a different clone than M3 but derived from the same initial VM-M3 tumor. Enzymatic lactate measurements were greater in M3II+ cells than M3II- cells when corrected to ATP levels (Figure 18B), suggesting that a decrease in respiration occurred in conjunction with an increase in fermentation. Ultimately, cellular assays done with mycoplasma-infected cell cultures need to be corrected by multiple parameters unless mycoplasma protein amount can be accurately separated from cellular protein amount in the assay being performed. Nonetheless, the possibility exists that in the present study *M. arginini* is interfering with lactate production when corrected to the milligram of cellular protein.

Possible mechanism of *M. Arginini*-induced diminished respiration.

The mechanism behind the decline in respiration by the *M. arginini* effect on M3+ cells is unknown. It seems clear that the diminished respiration by the *M. arginini* effect involves activation of M3 macrophage cells since *M. arginini* is capable of activating macrophages (*70*). Both *M. arginini*-activated and LPS-activated macrophages have been shown to release NO (*70*) (*71*) and other mycoplasma species can also induce NO release in macrophage cells (*91*). NO is a powerful respiratory inhibitor (*92*). Activated macrophages have been shown to severely diminish the respiration of six different cancer cell lines during co-culture, however the implications of NO were not discussed (*93*). In addition, activated macrophages are capable of injuring neurons partly through NO production, possibly diminishing neuronal respiration (*71*). Therefore activated macrophage metabolism in-vitro is sufficient to diminish the respiration system of co-cultured cells, partly do to NO

production. If activated macrophages can diminish the respiration of co-cultured cells then it should be possible that they are at the same time diminishing their own respiration in-vitro. Thus, perhaps the diminished respiration in M3+ cells is in part self-promoted by activation-induced NO production. If this scenario were true, it would mean that *M. arginini* activates M3+ cells and as a result M3+ cells produce NO that diminishes their own respiration as well as the respiration of neighboring M3+ cells. It has indeed been shown that activated macrophages experience a diminished respiration in-vitro (*65*) (*66*), but it is unclear whether the diminished respiration is a natural part of macrophage activation-induced catabolism or is rather an effect from an inflammatory secreted molecules such as NO or TNF-α (TNF-α also disrupts respiratory energy production (*94*)).

Potential mechanism of *M. arginini*-induced tumor progression

As mentioned above, the present study suggests that the presence of *M. arginini* leads to activation of M3 cells, a concomitant inflammatory response, and a diminished respiration. As tumor-promoting inflammation is an enabling characteristic of the hallmarks of cancer and deregulation of cellular energetics is an emerging hallmark of cancer, NO and TNF-α production by M3+ cells is perhaps leading to their diminished respiration. *M. arginini* induced inflammation in vivo is partly a probable cause of the tumor progression increase seen when inoculating M3+ cells in-vivo compared to M3- cells.

Therapeutic Implications

Mycoplasmas can be detected in a high percentage of a wide variety of primary human cancers (*42*) (*43*) (*44*) (*45*). Some mycoplasma species can cause cells in culture to be tumorigenic but studies injecting these species into animals and assessing any cancer causing potential or cancer promoting potential are lacking. However, mycoplasmas enable many of the hallmarks of cancer (*5*) (*31*) (*32*) (*24*) (*33*) (*34*) (*35*) (*37*) (*38*) (*39*) (*40*), and thus mycoplasma-targeted therapies could offer relief from progression and thus more time to patients with mycoplasma-infected cancers. For example, 55% of glioblastoma specimens (out of 35) tested positive for cytomegalovirus (*95*) and when antivirals against cytomegalovirus were given to glioblastoma patients, survival significantly improved (*96*). Interestingly, cytomegalovirus induces bio-energetic changes reminiscent of *M. arginini* infection in M3 cells (*97*) (*98*) (*99*). The present study warrants further investigation into the role mycoplasmas play in human cancer and to the extent in which mycoplasma infections present in human cancer. If mycoplasmas are found to play a major causative or provocative role in human cancer in a variety of cancers, mycoplasma-targeted therapies could prove efficacious in prevention of cancer and prolonging mycoplasma-infected patient survival.

Figure 1. Eradication of Mycoplasma Infection in VM-M3 cells. (A) A 1.5% agarose gel with amplified DNA products which include a positive control (+cont), the infected M3 cells (M3+), the eradicated M3 cells (M3—) and the negative control (cell growth media). The top band at 570 bp is an amplified Human / Mammalian-specific DNA sequence controlling for the presence of human or mammalian cells. The 260 bp band is the amplified extracted 16S rDNA gene capable of identifying 182 Mycoplasma species. The lower faint band is an amplified internal control band of an artificial gene derived from the human TNFα gene. MycoZap (Lonza) and a subsequent treatment with ciprofloxacin were used to eradicate the infection (M3—). The positive control is amplified extracted DNA from *Mycoplasma fermentans* infected K562 cells. The negative control is fresh DMEM high glucose plus 10%FBS. (B) The eradication was stable for up to three weeks in culture without the use of prophylactic methods.

Figure 1

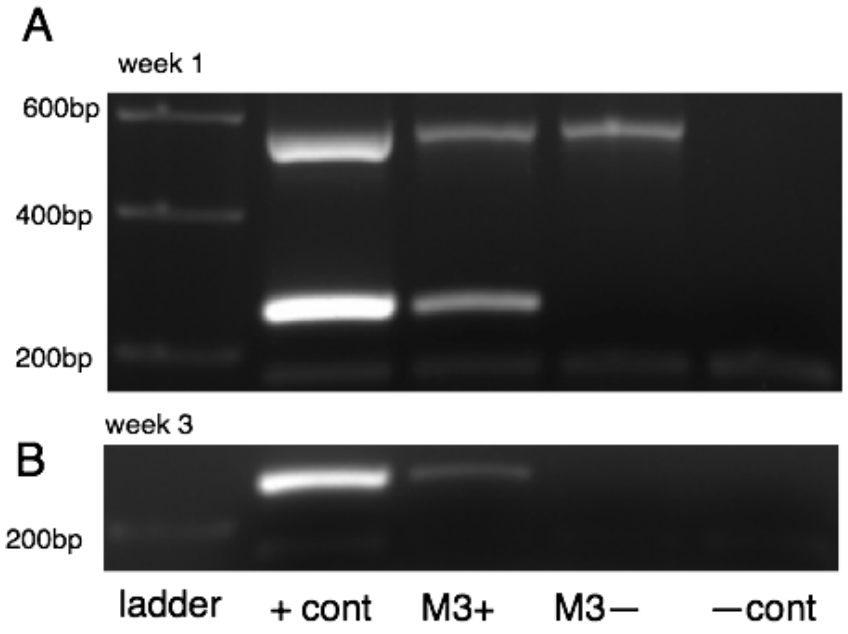
A
week 1
600bp
400bp
200bp
week 3
B
200bp
ladder
+ cont
M3+
M3—
—cont

Figure 2. Infection of VM-M3 cells by *Mycoplasma arginini*. (A) The sequenced DNA code of the excised 260 bp amplified band of mycoplasmal 16S rDNA of the M3+ cells. The mycoplasmal 16S rDNA sequence (query) was blasted and the best match (subject) was *Mycoplasma arginini*. Red stars indicate a mismatch or gap in the query compared to that of the subject. (B) The query rDNA sequence was aligned with a closely phylogenetic related species, i.e. *Mycoplasma hominis*, verifying the query rDNA sequence does not closely match other related mycoplasma species (6 red stars for *M. hominis* and 1 for *M.arginini*).

Figure 2

A

Mycoplasma arginini strain CBER2012BHK clone 3 16S ribosomal RNA gene, partial sequence

Sequence ID: gb|JQ903580.1| Length: 1500 Number of Matches: 1

Range 1: 802 to 1011 GenBank Graphics Next Match Previous Match

Score	Expect	Identities	Gaps	Strand
383 bits(207)	4e-103	209/210(99%)	0/210(0%)	Plus/Plus

```
Query  5    ACGATGATCATTAGTCGGTGGAGAGTTCACTGACGCAGCTAACGCATTAAATGATCCGCC  64
            ||||||||||||||||||||||||||||||||||||||||||||||||||||||||||||
Sbjct  802  ACGATGATCATTAGTCGGTGGAGAGTTCACTGACGCAGCTAACGCATTAAATGATCCGCC  861

Query  65   TGAGTAGTATGCTCGCAAGAGTGAAACTTAAAGGAATTGACGGGGACCCGCACAAGCGGT  124
            ||||||||||||||||||||||||||||||||||||||||||||||||||||||||||||
Sbjct  862  TGAGTAGTATGCTCGCAAGAGTGAAACTTAAAGGAATTGACGGGGACCCGCACAAGCGGT  921

Query  125  GGAGCATGTGGTTTAATTTGAAGATACGCGGAGAACCTTACCCACTCTTGACATCCTTCG  184
            ||||||||||||||||||||||||||||||||||||||||||||||||||||||||||||
Sbjct  922  GGAGCATGTGGTTTAATTTGAAGATACGCGGAGAACCTTACCCACTCTTGACATCCTTCG  981

Query  185  CAATGCTATAGAGATATAGAGGAGGTTAAC  214
            |||||||||||||||||| ||||||||||
Sbjct  982  CAATGCTATAGAGATATAGCGGAGGTTAAC  1011
```

* Mismatch or gap

B

Mycoplasma hominis ATCC 23114 strain PG21 16S ribosomal RNA gene, partial sequence; ribosomal RNA gene, partial sequence

Sequence ID: gb|JN935871.1| Length: 1523 Number of Matches: 1

Range 1: 782 to 988 GenBank Graphics Next Match Previous Match

Score	Expect	Identities	Gaps	Strand
350 bits(189)	4e-93	202/208(97%)	1/208(0%)	Plus/Plus

```
Query  5    ACGATGATCATTAGTCGGTGGAGAGTTCACTGACGCAGCTAACGCATTAAATGATCCGCC  64
            |||||||||||||||||||||||  ||||||||||||||||||||||||||||||||||
Sbjct  782  ACGATGATCATTAGTCGGTGGAGA-ATCACTGACGCAGCTAACGCATTAAATGATCCGCC  840

Query  65   TGAGTAGTATGCTCGCAAGAGTGAAACTTAAAGGAATTGACGGGGACCCGCACAAGCGGT  124
            ||||||||||||||||||||||||||||||||||||||||||||||||||||||||||||
Sbjct  841  TGAGTAGTATGCTCGCAAGAGTGAAACTTAAAGGAATTGACGGGGACCCGCACAAGCGGT  900

Query  125  GGAGCATGTGGTTTAATTTGAAGATACGCGGAGAACCTTACCCACTCTTGACATCCTTCG  184
            ||||||||||||||||||||||||||| |||| ||||||||||||||||||||||||||||
Sbjct  901  GGAGCATGTGGTTTAATTTGAAGATACACGGAAAACCTTACCCACTCTTGACATCCTTCG  960

Query  185  CAATGCTATAGAGATATAGAGGAGGTTA  212
            ||| |||||||||||||| ||||||||
Sbjct  961  CAAAGCTATAGAGATATAGTGGAGGTTA  988
```

Figure 3. Energy catabolism in mammalian cells. Energy Catabolism in mammalian cells is comprised from respiration (oxidative phosphorylation) and lactate fermentation. Pyruvate, fatty acids, amino acids, and the malate-aspartate shuttle all provide NADH to power oxidative phosphorylation (OXPHOS), The glycerol-3-phosphate shuttle and succinate provide FADH2 to power OXPHOS. NADH and FADH2 transfer high-energy electrons to the electron transport chain (Complexes I through IV) in which oxygen is the final low energy electron acceptor. The energy harnessed from high-energy electron transfer by complexes I through IV is used to pump protons into the inter membrane space creating a proton gradient that flows back into the mitochondrial matrix while ATP is synthesized by complex V. Normal mammalian cells derive the major percentage of their energy through respiration with lactate fermentation rarely providing over 20% of energy needs. If energy through respiration is limited by hypoxia or pharmacological inhibition, lactate fermentation will increase in attempts to compensate for the lost respiratory energy. It is unclear if and in what cell types fermentation energy can completely replace the loss of all respiratory energy. Respiration is classically measured by oxygen consumption and lactate fermentation through lactate production. Accepted values are 5 moles of ATP produced for every mole of oxygen consumed and 1 mole of ATP for every mole of lactate produced.

Figure 3

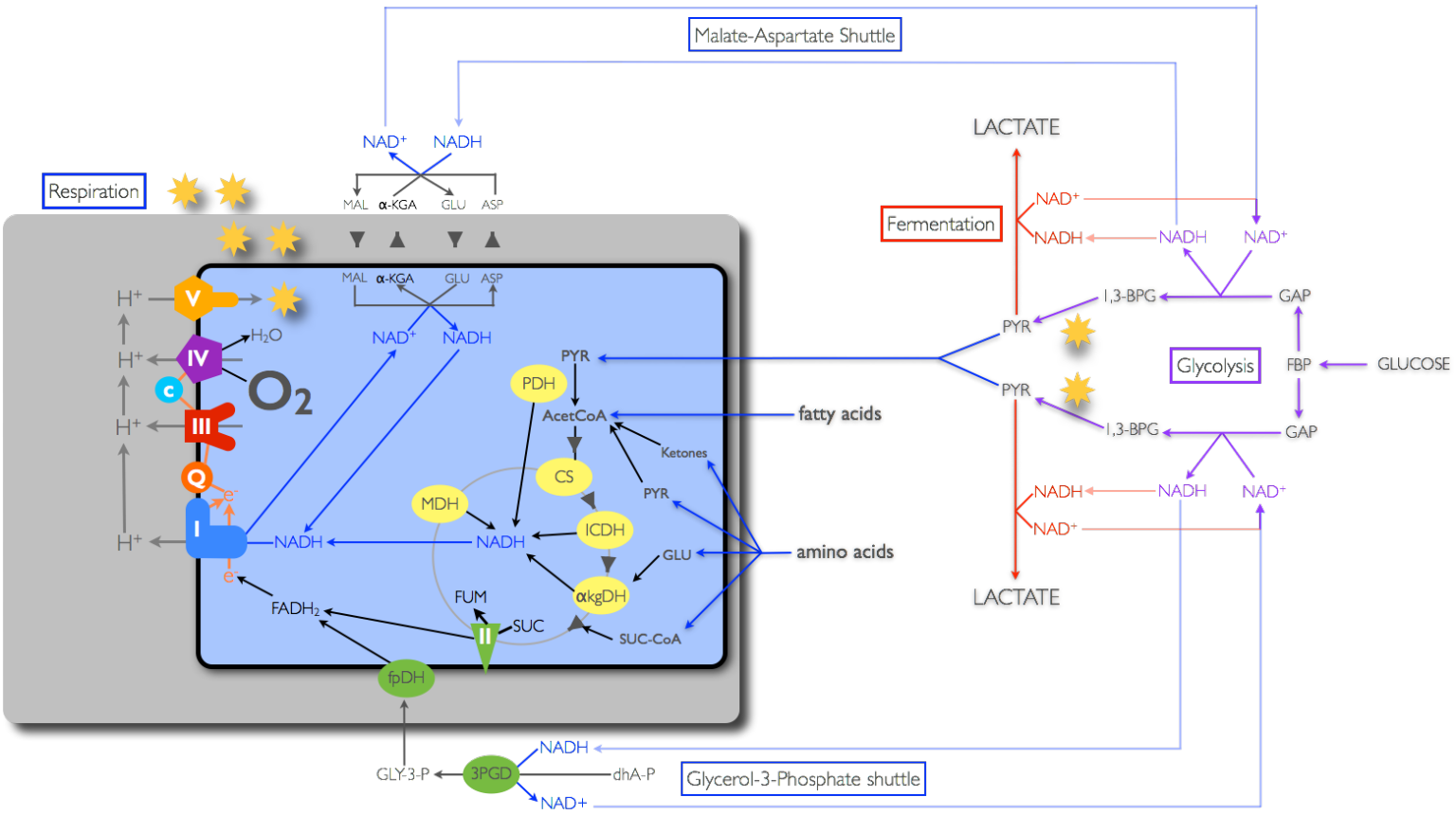
Malate-Aspartate Shuttle
NAD+
NADH
MAL
α-KGA
GLU
ASP
Respiration
LACTATE
Fermentation
NAD+
NADH
NADH
NAD+
1,3-BPG
GAP
PYR
Glycolysis
FBP
GLUCOSE
PYR
1,3-BPG
GAP
NADH
NADH
NAD+
NAD+
LACTATE
H+
V
H2O
IV
O2
c
III
Q
I
e-
PDH
AcetCoA
fatty acids
Ketones
CS
MDH
PYR
ICDH
NADH
NADH
GLU
amino acids
αkgDH
FUM
FADH2
II
SUC
SUC-CoA
fpDH
GLY-3-P
3PGD
NADH
dhA-P
NAD+
Glycerol-3-Phosphate shuttle

Figure 4. Measurement of energy catabolism with a Seahorse XF-96 Flux Analyzer. (A) A picture of the Seahorse XF-96 Flux Analyzer unit is shown with a 96-well plate loaded in the retractable slot on the right. The Seahorse XF-96 used in the studies within this thesis resides at Berg Pharma. (B) A cartoon side-view of two individual wells of a Seahorse XF96 specific 96-well plate. To the left of the boxed number 1, cells (green spheres) can be seen on the bottom of the well. Boxed number 2 represents the oxygen (orange) and pH (blue) measurement probes that rise up and dip down into the media (pink) of the incubating cells. Boxed number 3 shows drug-dispensing ports that can inject drugs of choice into the media at specified times. (C) During oxygen and pH measurements the probe travels down to create an air tight compartment right above the cells (7 ul of volume total). When the sensor probes are completely down a closed system is created in which oxygen rate can be assessed. To prevent hypoxic conditions, after a short measurement is complete (7 minutes in this study), the probe travels back up (as in B) to allow the oxygen, pH, and nutrients to re-equilibrate.

Figure 4

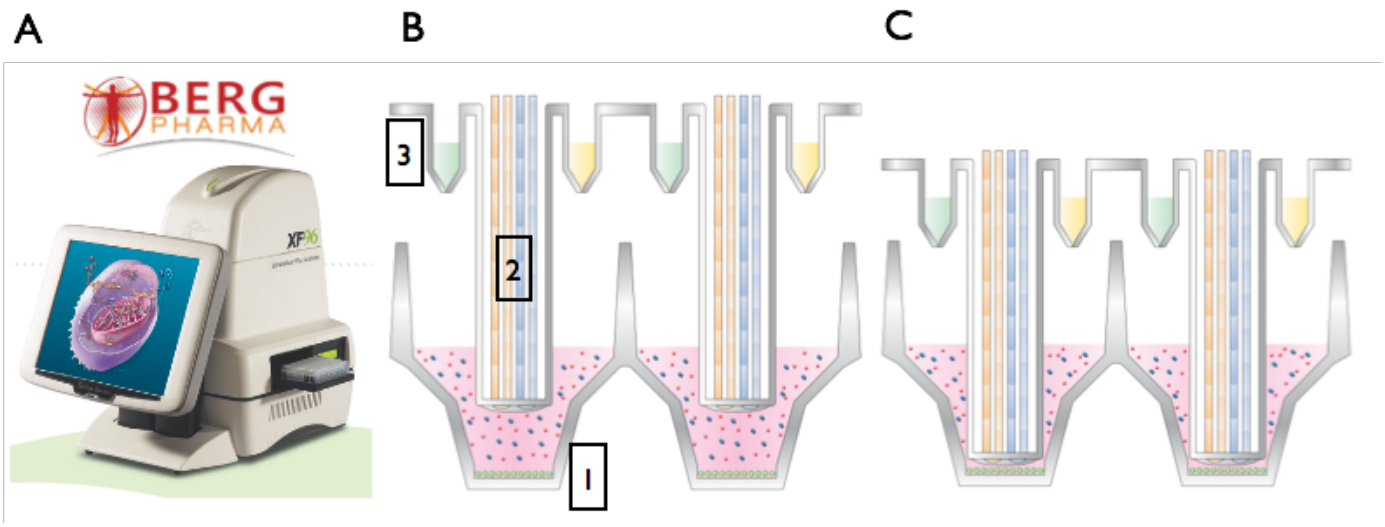

Figure 5. Comparison of oxygen consumption, ECAR, and lactate production of M3+ and M3— cells in the presence and absence of Antimycin A. Oxygen consumption rate (A) Extracellular acidification rate (ECAR) (B), and Lactate production rate (C) in M3+ and M3— cells. Complete media is DMEM with 2 mM glutamine, 10 mM glucose, and 0.5 mg/mL Albumax I. No FBS and no bicarbonate was included as recommended by Seahorse for ECAR measurements. Phenol red was not included since visual pH monitoring was unnecessary. The concentration of Antimycin A was 100 nM. Oxygen consumption, ECAR, enzymatic lactate, and protein were all measured from the same well using a Seahorse XF96 Analyzer. In the —Antymycin A condition n=8 and in the + Antymycin A condition n=4. Error bars represent 95% confidence intervals calculated using Excel. * = $p < 0.05$ ** = $p < 0.01$ (determined by the two tailed student t-test).

Figure 5

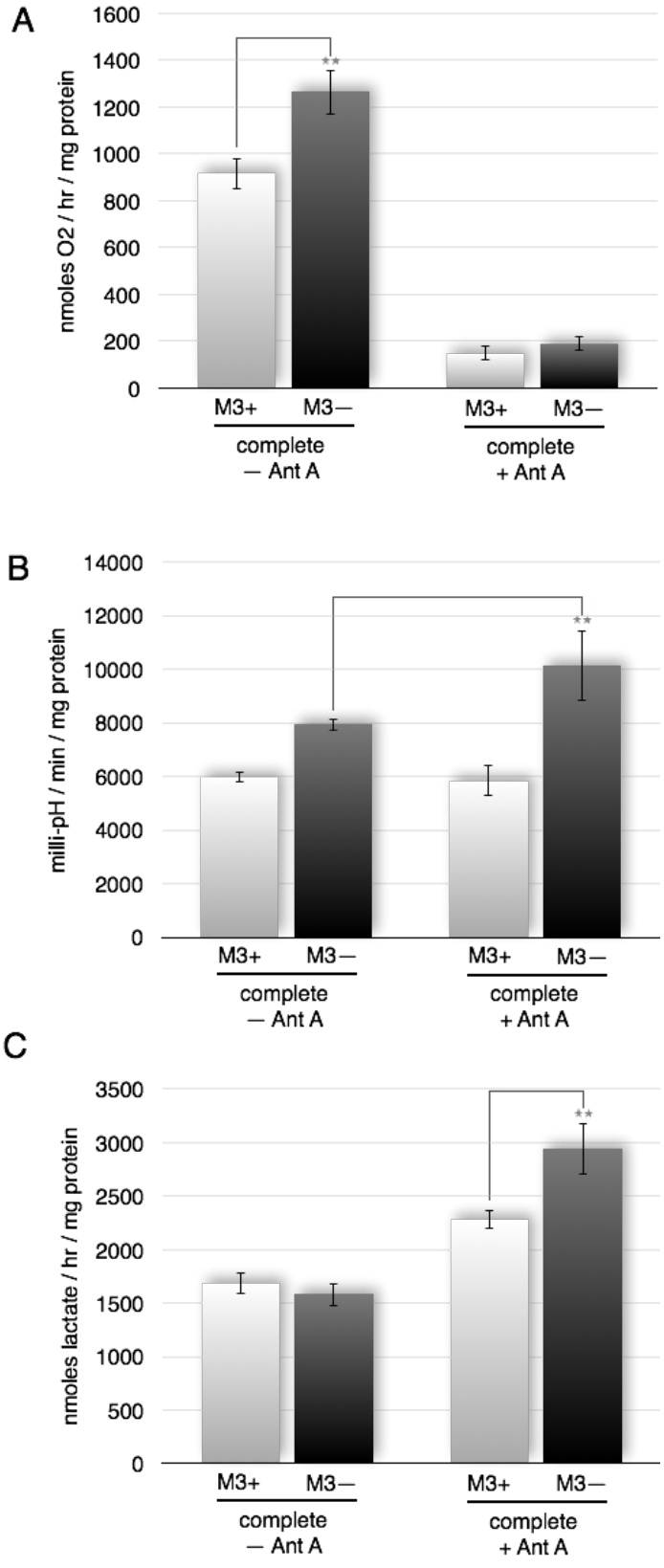
A
nmoles O2 / hr / mg protein
1600
1400
1200
1000
800
600
400
200
0
**
M3+
M3—
complete
— Ant A
M3+
M3—
complete
+ Ant A
B
milli-pH / min / mg protein
14000
12000
10000
8000
6000
4000
2000
0
**
M3+
M3—
complete
— Ant A
M3+
M3—
complete
+ Ant A
C
nmoles lactate / hr / mg protein
3500
3000
2500
2000
1500
1000
500
0
**
M3+
M3—
complete
— Ant A
M3+
M3—
complete
+ Ant A

Figure 6. Lactate production of infected and eradicated M3 and M3II cells (A) Relative area of extracellular lactate in the media after 6 hours of incubation with M3+ or M3— cells in normal air. Metabolomic analysis was performed by Human Metabolome Technologies (HMT) using Capillary Electrophoresis Time-of-Flight Mass Spectrometry. All metabolomic analysis was done with an n=4. Error bars represent 95% confidence intervals calculated using Excel. (B) Millimoles of lactate in media measured enzymatically after 48 hours of incubation in an airtight Coy Laboratory Chamber. The percentage of gas was set at 20% oxygen, 5% CO2, and 75% N2. The graph represents the lactate production after 48 hours incubation corrected to ATP levels also taken at 48hrs (n=5). Error bars represent 95% confidence intervals calculated using Excel. * = $p < 0.05$ ** = $p < 0.01$ *** = $p < 0.001$

Figure 6

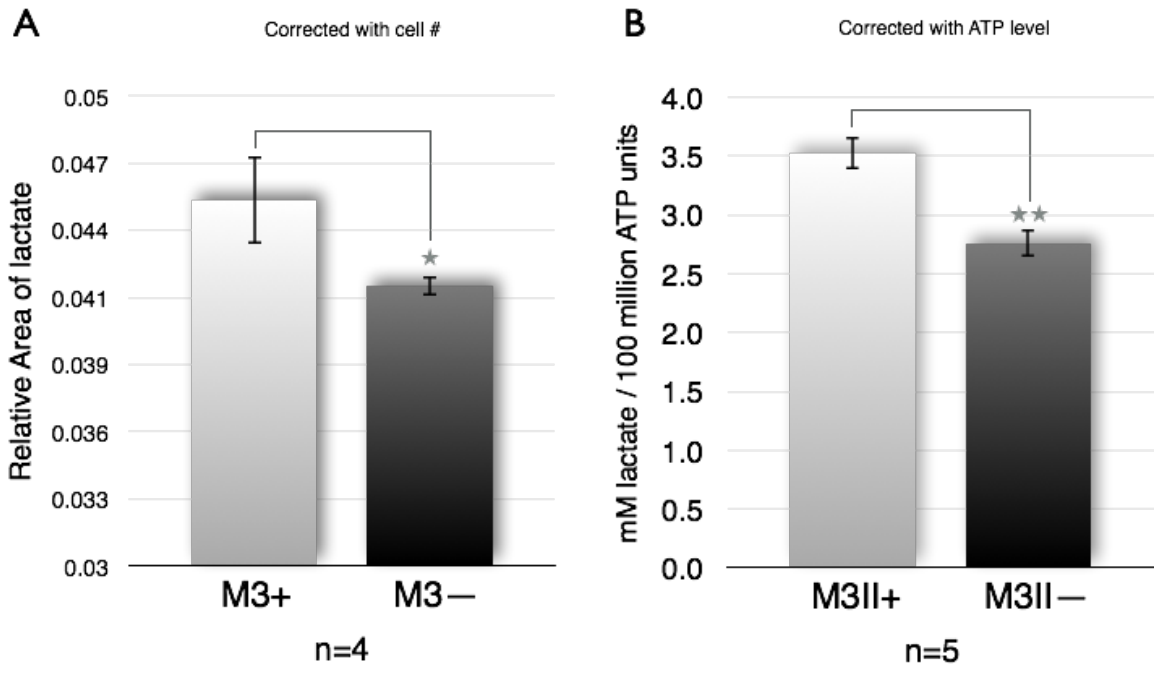
A
Corrected with cell #
Relative Area of lactate
0.05
0.047
0.044
0.041
0.039
0.036
0.033
0.03
M3+
M3—
n=4
B
Corrected with ATP level
mM lactate / 100 million ATP units
4.0
3.5
3.0
2.5
2.0
1.5
1.0
0.5
0.0
M3II+
M3II—
n=5

Figure 7. LDHA and Cytochrome c Oxidase protein expression of M3+ and M3— cells. (A) Western blot (fluorescent secondary) of the M subunit of the Lactate Dehydrogenase enzyme encoded by the LDHA gene. (B) Western Blot (fluorescent secondary) of protein subunit IV of the Cytochrome c Oxidase protein. (C) Quantification of LDHA to B-Actin levels in M3+ versus M3— cells. (D) Quantification of Cytochrom C Oxidase to B-Actin levels in M3+ versus M3— cells. n=3 for A-D. Error bars represent 95% confidence intervals calculated using Excel.

Figure 7

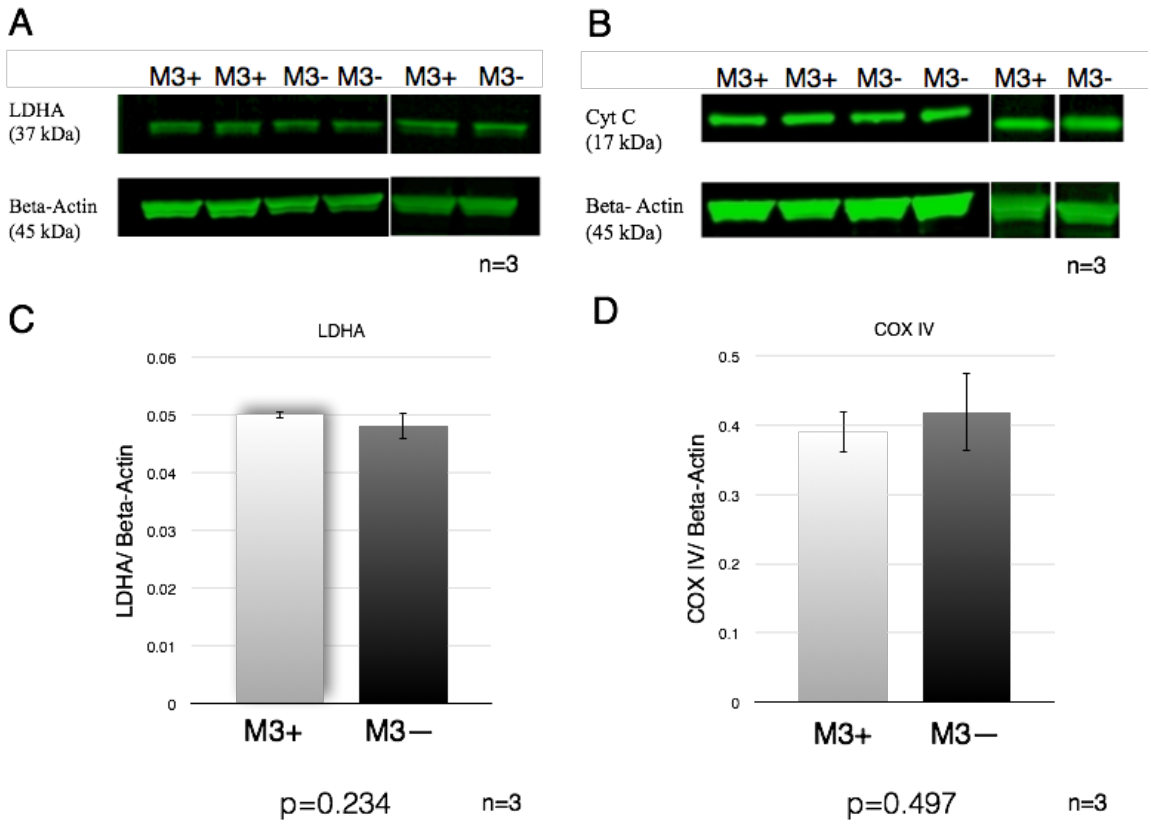
A
M3+ M3+ M3- M3- M3+ M3-
LDHA
(37 kDa)
Beta-Actin
(45 kDa)
n=3
B
M3+ M3+ M3- M3- M3+ M3-
Cyt C
(17 kDa)
Beta- Actin
(45 kDa)
n=3
C
LDHA
LDHA/ Beta-Actin
0.06
0.05
0.04
0.03
0.02
0.01
0
M3+
M3—
p=0.234
n=3
D
COX IV
COX IV/ Beta-Actin
0.5
0.4
0.3
0.2
0.1
0
M3+
M3—
p=0.497
n=3

Figure 8. The influence of glucose on the oxygen consumption of M3+ and M3 — cells. (A) Oxygen consumption rate of M3+ and M3— cells grown in the absence or presence of glucose (10mM) in media containing amino acids and fatty acids.(B) In order to quantify the Crabtree effect the % Crabtree effect equation was utilized from "Pasteur and Crabtree effects - Assays in cells, Wenner 1979". Q_{O2} = the nmoles of O_2 consumed / hr / mg protein. Quantification of the % Crabtree effect is shown in table 1. n=8 for both —glc and +glc conditions for M3+ and M3— cells. Error bars represent 95% confidence intervals calculated using Excel. * = $p < 0.05$ ** = $p < 0.01$ (determined by the two tailed student-test).

Figure 8

A

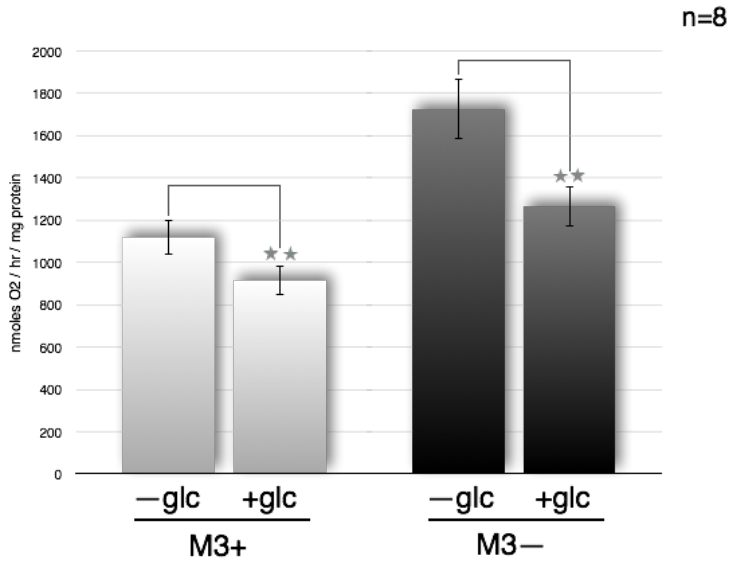

B

$$\%\ Crabtree\ effect = \left(\frac{Q_{O2}\ no\ glc\ media - Q_{O2}\ glc\ media}{Q_{O2}\ no\ glc\ media}\right)(100)$$

Table 1

Table 1. Calculating the % Crabtree effect from respiration rate in the presence and absence of glucose.

	M3+			M3—		
	+ glc	**—glc**	**equation**	**+ glc**	**—glc**	**equation**
Respiration Rate (RR) nmoles O2- / hr / mg protein	767	971	$\frac{971 - 767}{971}$	1,073	1,535	$\frac{1,535 - 1,073}{1535}$
% Crabtree effect		21%			30%	

Values taken from respiration rates from graph of Figure 5 with subtraction of the Antimycin A insensitive respiration.
% Crabtree effect equation modified from: Pasteur and Crabtree effects - Assays in cells. Wenner 1979.

Figure 9. Production of Itaconic acid by M3+ and M3- cells. Relative area of intracellular isocitrate, intracellular itaconic acid, and extracellular itaconic acid in the media after 6 hours of incubation with M3+ or M3— cells. Control media had no cells but was incubated for the 6 hour period. Itaconic acid is a bactericidal metabolite produced by activated macrophages. Rather than cis-aconitate producing isocitrate, activated macrophages seem to use cis-aconitate to produce itaconic acid. Metabolomic analysis was performed by Human Metabolome Technologies (HMT) using Capillary Electrophoresis Time-of-Flight Mass Spectrometry. All metabolomic analysis was done with an n = 4. Error bars represent 95% confidence intervals calculated using Excel. * = $p < 0.05$ ** = $p < 0.01$.

Figure 9

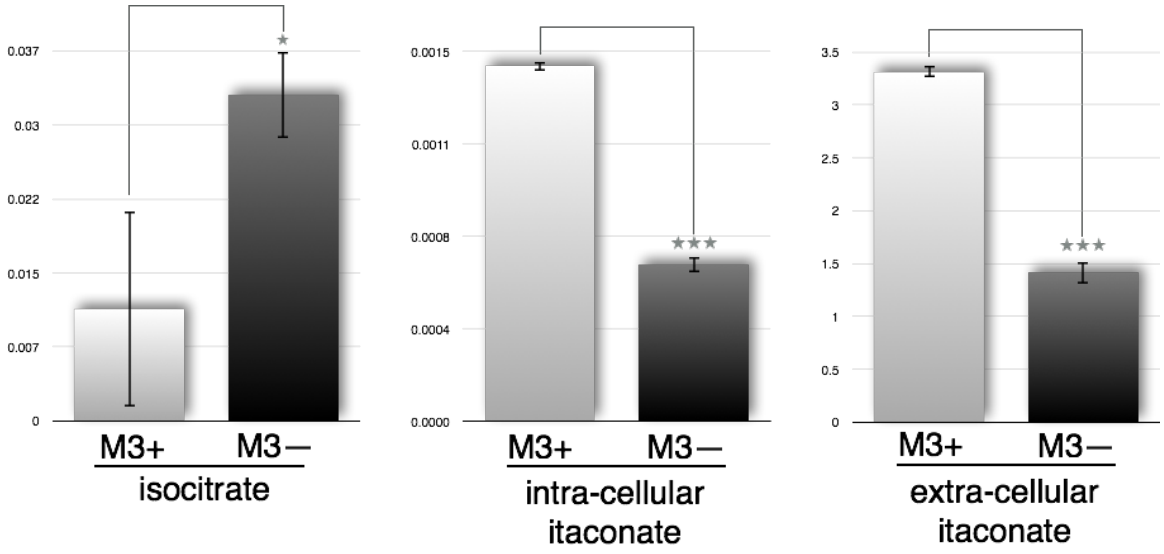
0.037
0.03
0.022
0.015
0.007
0
M3+
M3—
isocitrate
0.0015
0.0011
0.0008
0.0004
0.0000
M3+
M3—
intra-cellular
itaconate
3.5
3
2.5
2
1.5
1
0.5
0
M3+
M3—
extra-cellular
itaconate

Figure 10. Production of succinate via the GABA shunt by M3+ and M3- cells. Relative area of intracellular GABA, intracellular succinate, and extracellular succinate in cell extractions or in the media after 6 hours of incubation with M3+ or M3— cells. Control media had no cells but was incubated for the 6 hour period. Itaconic acid is a bactericidal metabolite produced by activated macrophages. Metabolomic analysis was performed by Human Metabolome Technologies (HMT) using Capillary Electrophoresis Time-of-Flight Mass Spectrometry. All metabolomic analysis was done with an n = 4. Error bars represent 95% confidence intervals calculated using Excel. * = $p < 0.05$ ** = $p < 0.01$ *** = $p < 0.001$

Figure 10

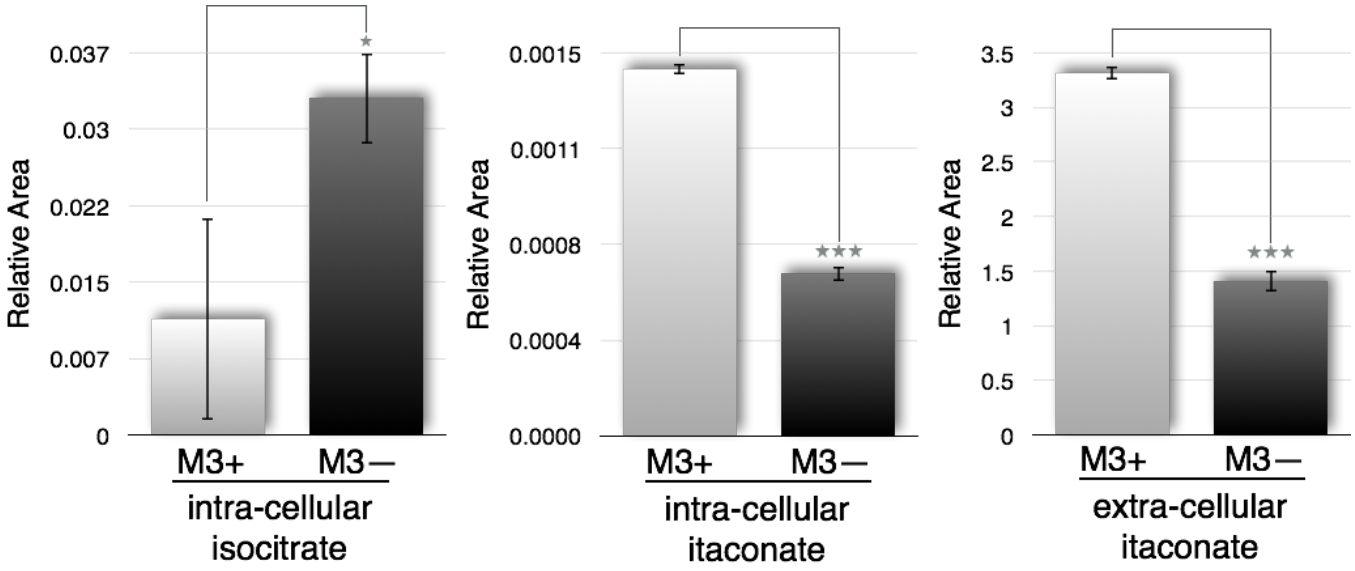
Relative Area
0.037
0.03
0.022
0.015
0.007
0
M3+
M3—
intra-cellular
isocitrate
Relative Area
0.0015
0.0011
0.0008
0.0004
0.0000
M3+
M3—
intra-cellular
itaconate
Relative Area
3.5
3
2.5
2
1.5
1
0.5
0
M3+
M3—
extra-cellular
itaconate

Figure 11. Production of Citrulline from Arginine in M3+ and M3- cells.

Relative area of L-arginine and citrulline in extracted intra-cellular metabolites of M3+ and M3— cells incubated in complete media for 6 hours. The relative area of citrulline in the M3— condition is at 0.004, however the bar is not visible in the graph. Activated macrophages produce Nitric Oxide by metabolizing arginine to citrulline. Metabolomic analysis was performed by Human Metabolome Technologies (HMT) using Capillary Electrophoresis Time-of-Flight Mass Spectrometry. All metabolomic analysis was done with an n = 4. Error bars represent 95% confidence intervals calculated using Excel. * = $p < 0.05$ ** = $p < 0.01$.

Figure 11

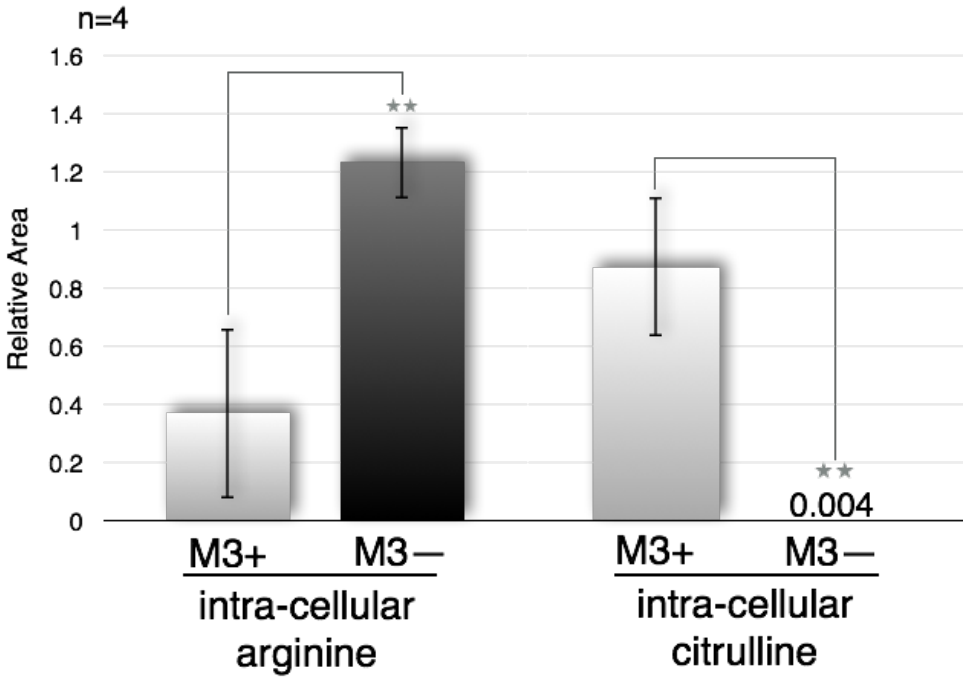
n=4
Relative Area
1.6
1.4
1.2
1
0.8
0.6
0.4
0.2
0
0.004
M3+
M3—
intra-cellular arginine
M3+
M3—
intra-cellular citrulline

Figure 12. Pentose Phosphate Pathway metabolism in M3+ and M3— cells. (A) Relative area of intra-cellular Ribose-5-Phosphate (R5P), Ribulose-5-Phosphate (Ru5P), and Phosphoribosyl Pyrophosphate (PRPP). The pentose phosphate pathway provides intermediates for growth. Metabolomic analysis was performed by Human Metabolome Technologies (HMT) using Capillary Electrophoresis Time-of-Flight Mass Spectrometry. All metabolomic analysis was done with an n = 4. Error bars represent 95% confidence intervals calculated using Excel * = $p < 0.05$ ** = $p < 0.01$ *** = $p < 0.001$

Figure 12

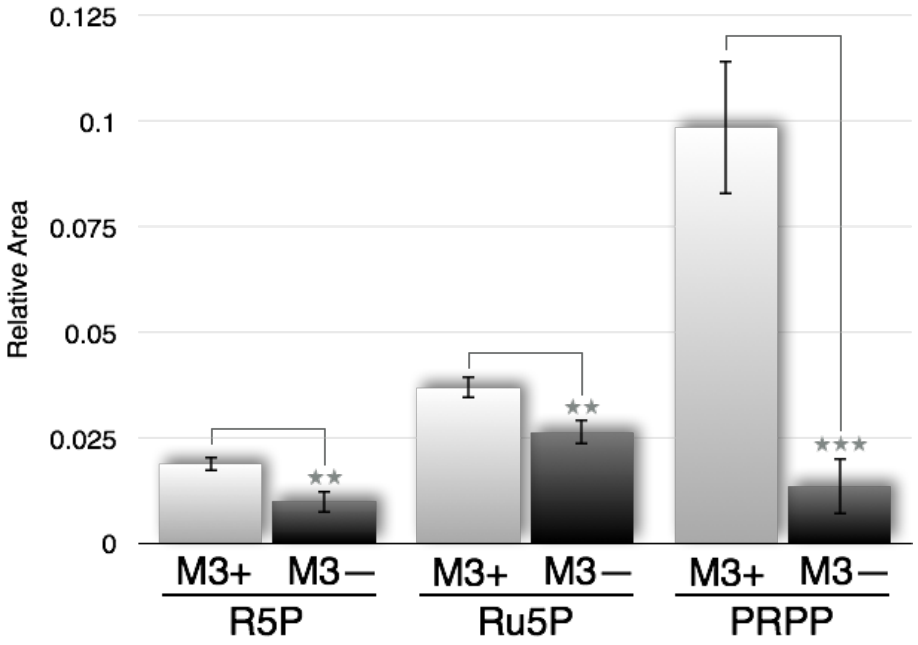
0.125
0.1
0.075
0.05
0.025
0
Relative Area
M3+
M3—
R5P
M3+
M3—
Ru5P
M3+
M3—
PRPP

Figure 13. Proliferation of M3+ and M3— cells in-vitro. (A) In-vitro proliferation over 2 days of M3+ and M3— cells seeded at 15,000 cells/well using an bioluminescent ATP assay (photons / second). (B) In-vitro proliferation over 5 days of M3+ and M3— cells seeded at 5,000 cell/well using a BCA protein assay. n=8 for both ATP and protein assays. Error bars represent 95% confidence intervals calculated using Excel.

Figure 13

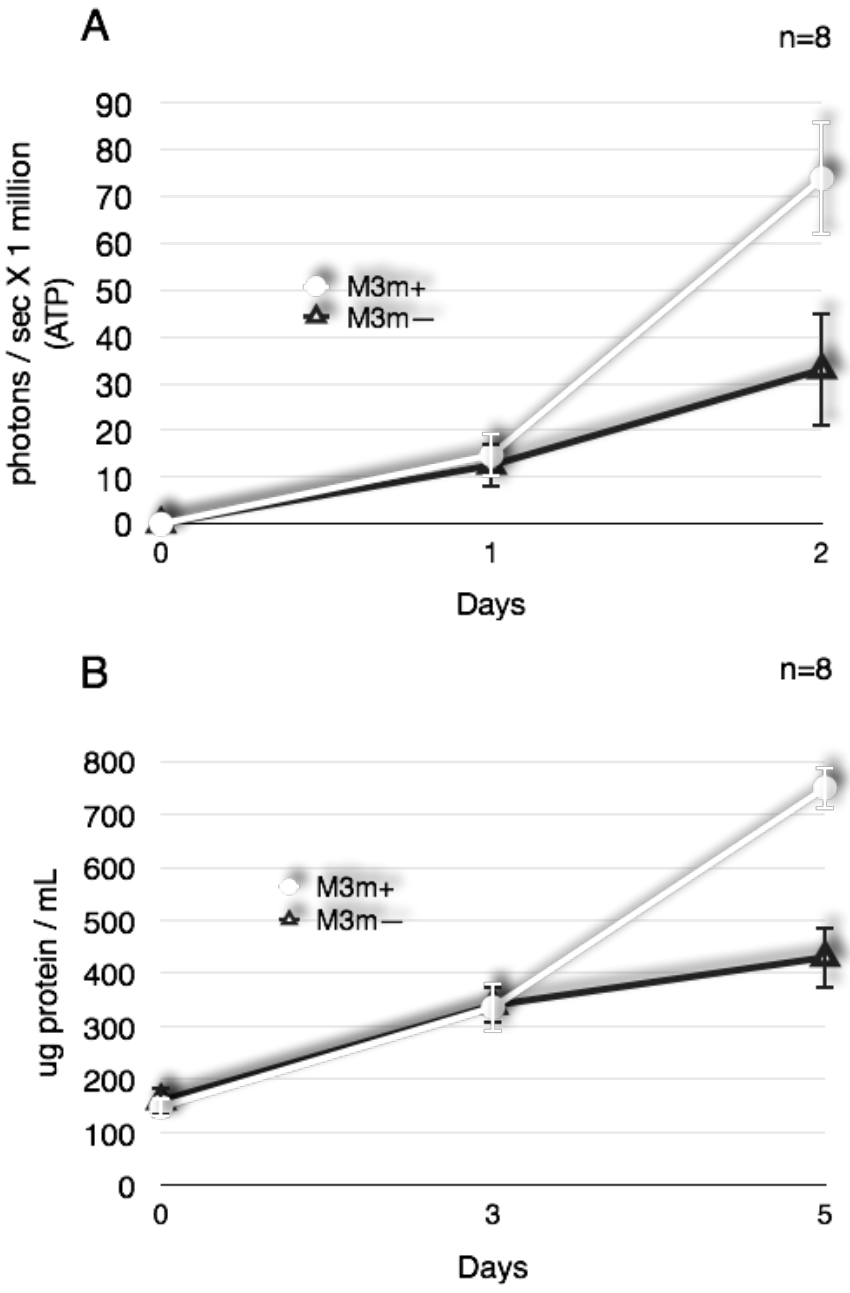
A
n=8
photons / sec X 1 million (ATP)
90
80
70
60
50
40
30
20
10
0
M3m+
M3m—
0
1
2
Days
B
n=8
ug protein / mL
800
700
600
500
400
300
200
100
0
M3m+
M3m—
0
3
5
Days

Figure 14. Primary tumor weights of inoculated M3+ and M3— cells in VM-mice. (A) In-vivo Experiment I - Primary tumor wet weight of 1.5 million M3+ and M3— cells injected subcutaneously in the back of three VM mice. (B) In-vivo experiment II - Primary tumor wet weight of 1.5 million M3+ and M3— cells injected subcutaneously in the flank of three VM mice. n=3 mice for both experiment I and II and n=3 for both M3+ and M3—. Error bars represent 95% confidence intervals calculated using Excel. * = $p < 0.05$ ** = $p < 0.01$.

Figure 14

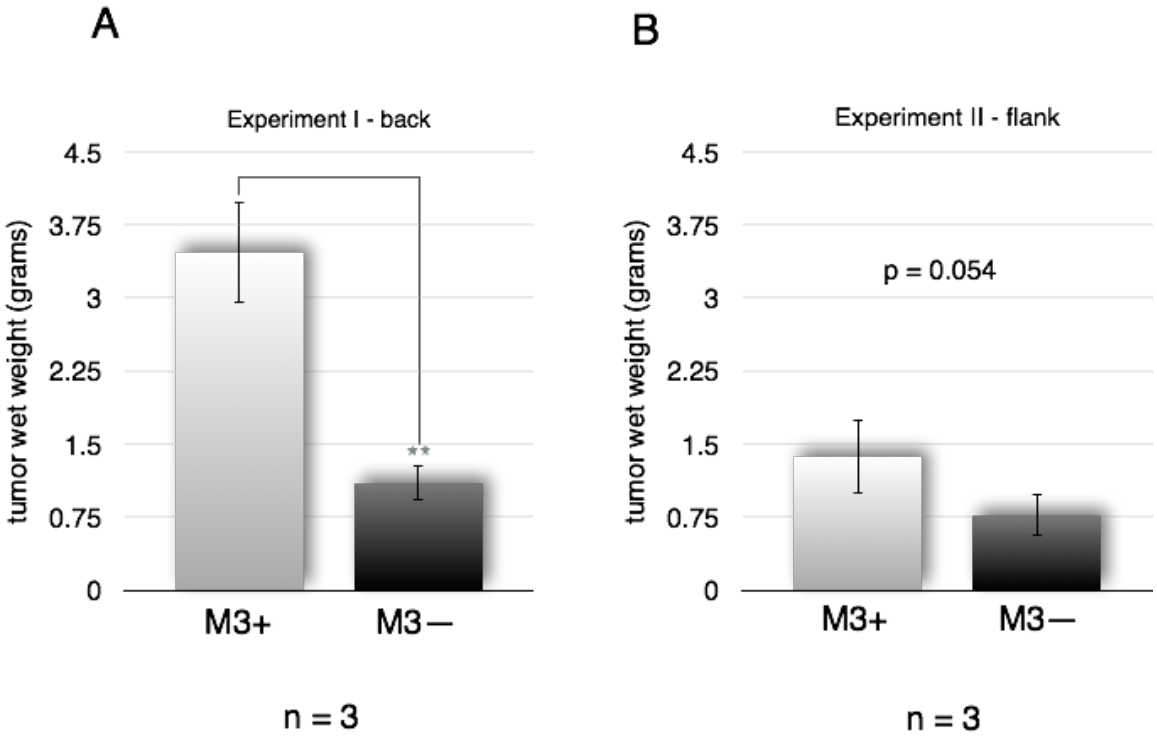
A
Experiment I - back
tumor wet weight (grams)
4.5
3.75
3
2.25
1.5
0.75
0
**
M3+
M3—
n = 3
B
Experiment II - flank
tumor wet weight (grams)
4.5
3.75
3
2.25
1.5
0.75
0
p = 0.054
M3+
M3—
n = 3

Figure 15. The VM mouse metastatic tumor model. (A) Tumors were implanted subcutaneously with VM-M3 cells and dorsal images were taken over 23 days. (B) Appearance of metastatic nodules in liver at 23 days in mice implanted subcutaneously with VM-M3 cells (first panel) compared to a normal control liver. Images were taken from: L. C. Huysentruyt, P. Mukherjee, D. Banerjee, L. M. Shelton, T. N. Seyfried, Metastatic cancer cells with macrophage properties: evidence from a new murine tumor model., Int. J. Cancer 123, 73–84 (2008).

Figure 15

A

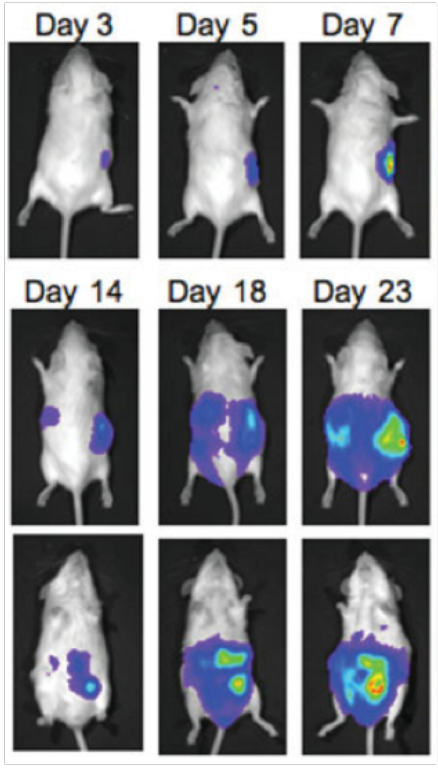

B

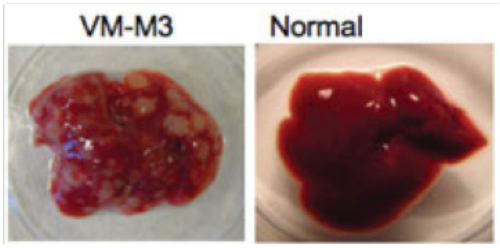

Figure 16. In-vitro luminescence output of M3+ and M3— cells. ATP bioluminescence assay for luciferase activity in M3+ and M3— cells in vitro using increasing concentrations of luciferin (substrate for luciferase). Progressive microgram amounts of luciferin were added to a 120ul of growth media with 30,000 cells / well in a 96-well plate. The bioluminescence output is based on intracellular concentrations of ATP, oxygen, and luciferin as well as luciferase activity. The data was normalized to milligram protein levels. n=8 in all conditions. Error bars represent 95% confidence intervals calculated using Excel.

Figure 16

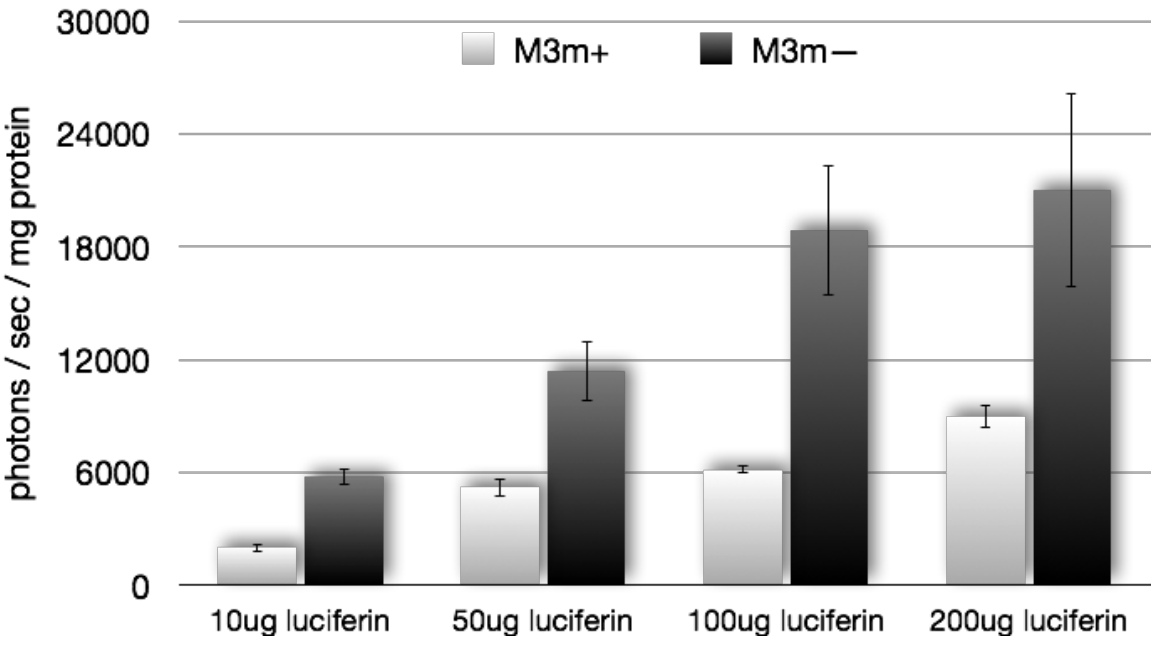
30000
24000
18000
12000
6000
0
photons / sec / mg protein
M3m+
M3m−
10ug luciferin
50ug luciferin
100ug luciferin
200ug luciferin

Figure 17. Assessment of metastatic spread in VM mice after inoculation with M3+ and M3- cells. Visual assessment of metastasis nodules in liver and ATP (photons / sec) assessment of metastasis to brain in M3+ and M3- inoculated mice from experiment II. M3+ and M3— cells are transfected with a firefly luciferase vector that emits light when in contact with luciferin, ATP, and oxygen. The brain was removed, incubated in a luciferin/PBS solution, and finally imaged for bioluminescence using a Xenogen IVIS Lumina system. The n=3 for experiment II as is seen by noting mouse 1, 2, and 3 in the figure for both M3+ and M3— conditions.

Figure 17

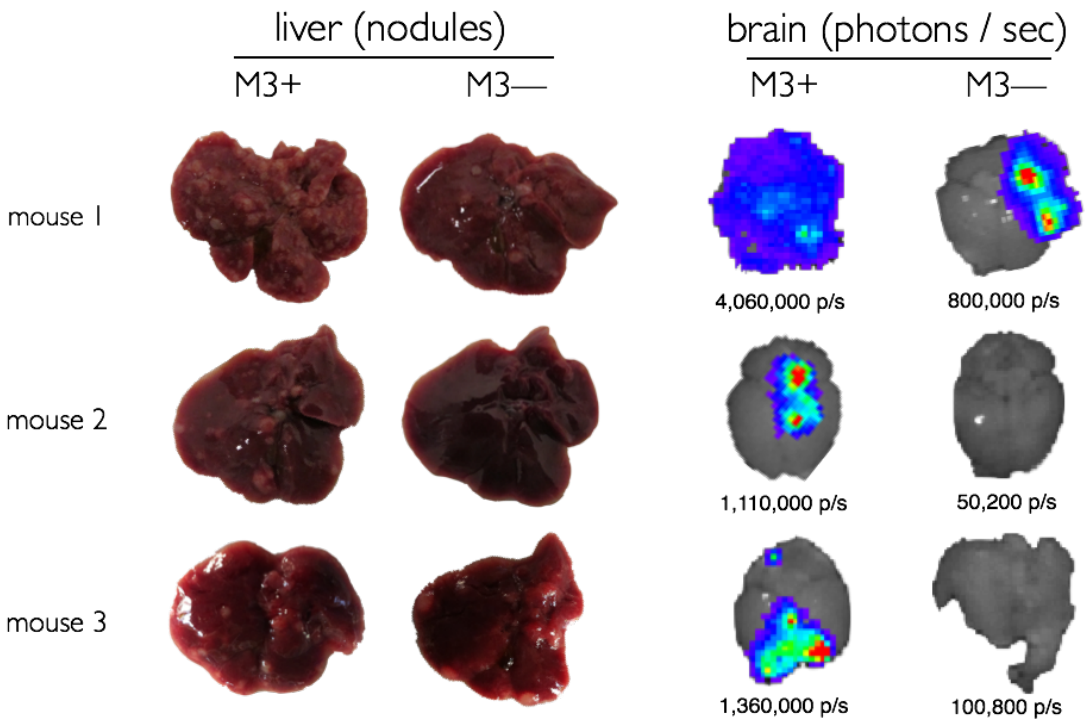
liver (nodules)
M3+
M3—
brain (photons / sec)
M3+
M3—
mouse 1
mouse 2
mouse 3
4,060,000 p/s
800,000 p/s
1,110,000 p/s
50,200 p/s
1,360,000 p/s
100,800 p/s

Figure 18. Reduced oxygen consumption is associated with enhanced metastasis in M3II+ and M3II- cells. (A) O2 consumption measurement taken using a Presens Sensor Dish Reader (SDR) in an airtight Coy Laboratory Chamber. The percentage of gas was set at 20% oxygen, 5% CO2, and 75% N2. The graph represents the percentage of O2 consumed at 48hrs relative to ATP levels also taken at 48hrs (n=5). Error bars represent 95% confidence intervals calculated using Excel. *** = p-value < 0.0001. (B) Two mice inoculated with 7 million M3II+ or M3II— cell 57 days prior to date of taking the bioluminescence image. The image shows emission of photons from luciferase transfected M3II+ and M3II— cells 10 minutes after injection of luciferin. The photons are made from the interaction of luciferin, ATP, and O2 with luciferase. Purple to red indicates low to high cell concentration, respectively. n=1 mouse for each MII3+ / M3II— condition. A survival date was taken when each mouse became morbid.

Figure 18

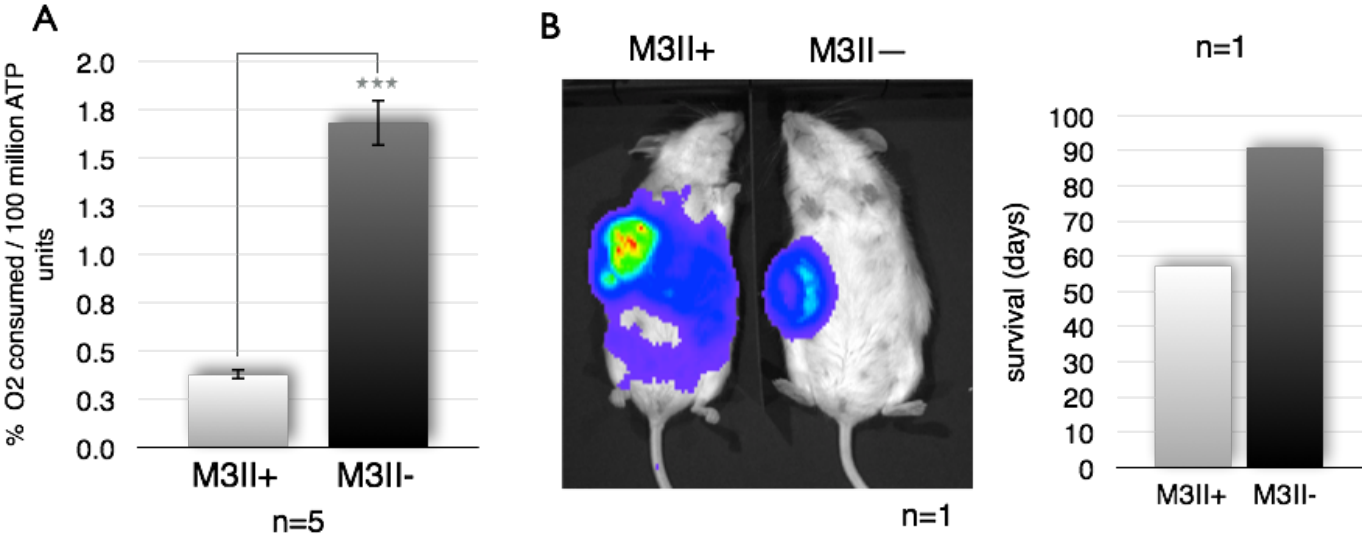
A
% O2 consumed / 100 million ATP units
2.0
1.8
1.5
1.3
1.0
0.8
0.5
0.3
0.0
***
M3II+
M3II-
n=5
B
M3II+
M3II—
n=1
n=1
survival (days)
100
90
80
70
60
50
40
30
20
10
0
M3II+
M3II-

References

1. G. Rawadi, O. Dussurget, Advances in PCR-based detection of mycoplasmas contaminating cell cultures., *PCR Methods Appl.* **4**, 199–208 (1995).

2. W. G. Weisburg *et al.*, A phylogenetic analysis of the mycoplasmas: basis for their classification., *J. Bacteriol.* **171**, 6455–67 (1989).

3. J. I. Glass *et al.*, Essential genes of a minimal bacterium., *Proc. Natl. Acad. Sci. U. S. A.* **103**, 425–30 (2006).

4. S. Razin, L. Hayflick, Highlights of mycoplasma research--an historical perspective., *Biologicals* **38**, 183–90 (2010).

5. S. Rottem, Interaction of mycoplasmas with host cells., *Physiol. Rev.* **83**, 417–32 (2003).

6. E. Stanbridge, Mycoplasmas and cell cultures., *Bacteriol. Rev.* **35**, 206–27 (1971).

7. C. Koch, J. Biaglow, Cyanide insensitive respiration in mammalian cells: an artifact of mycoplasmal contamination, *Adv. Exp. Med. Biol.* **159**, 337–45 (1983).

8. J. W. Choi, W. G. Haigh, S. P. Lee, Caveat: mycoplasma arginine deiminase masquerading as nitric oxide synthase in cell cultures., *Biochim. Biophys. Acta* **1404**, 314–20 (1998).

9. J. Denecke, K. Becker, H. Jurgens, R. Gross, J. E. A. Wolff, Falsification of Tetrazolium Dye (MTT) Based Cytotoxicity Assay Results due to Mycoplasma Conntamination of Cell Cultures, *Anticancer Res.* **19**, 1245–1248 (1999).

10. M. Gabridge, Metabolic consequences of mycoplasma pneumoniae infection, *Isr. J. Med. Sci.* **23**, 574–579 (1987).

11. M. Hopfe, R. Deenen, D. Degrandi, K. Köhrer, B. Henrich, Host cell responses to persistent mycoplasmas--different stages in infection of HeLa cells with Mycoplasma hominis., *PLoS One* **8**, e54219 (2013).

12. C. J. Miller *et al.*, Mycoplasma infection significantly alters microarray gene expression profiles., *Biotechniques* **35**, 812–4 (2003).

13. D. Niklas *et al.*, Mitochondrial activities in human cultured skin fibroblasts contaminated by Mycoplasma hyorhinis, *BMC Biochem.* **7**, 1–7 (2003).

14. J. D. Pollack, M. V Williams, R. N. McElhaney, The comparative metabolism of the mollicutes (Mycoplasmas): the utility for taxonomic classification and the relationship of putative gene annotation and phylogeny to enzymatic function in the smallest free-living cells., *Crit. Rev. Microbiol.* **23**, 269–354 (1997).

15. D. Voet, J. Voet, C. Pratt, *Fundamentals of Biochemistry: Life at the Molecular Level* (Wiley, ed. 4, 2012; http://www.lavoisier.fr/livre/notice.asp?ouvrage=1343423).

16. S. Smith, P. Van Demark, J. Fabricant, Respiratory pathways in the mycoplasma., *Ann. N. Y. Acad. Sci.* **143**, 77–84 (1967).

17. J. D. Pollack, A. J. Merola, M. Platz, R. L. Booth, Respiration-Associated Components of Mollicutes, **146**, 907–913 (1981).

18. R. Schimke, Studies on the metabolism of arginine by mycoplasma, *Ann. N. Y. Acad. Sci.* **143**, 573–577 (1967).

19. R. G. Hahn, G. E. Kenny, Differences in arginine requirement for growth among arginine-utilizing Mycoplasma species., *J. Bacteriol.* **117**, 611–8 (1974).

20. M. Barile, R. DelGiudice, T. Carski, C. Gibbs, J. Morris, Isolation and chatacterization of mycoplasma arginini: spec.nov., *Proc. …* **129**, 489–494 (1968).

21. P. Smith, Amino Acid Metabolism of PPLO, *Ann. N. Y. Acad. Sci.* **551**, 543–550 (1960).

22. R. Schimke, C. Berlin, The Generation of Energy by the Arginine Dihydrolase Pathway in Mycoplasma hominis 07, *J. Biol. Chem.* **241**, 2228–2236 (1966).

23. J. Baseman, Mycoplasmas: Sophisticated, Reemerging, and Burdened by Their Notoriety, *Emerg. Infect. Dis.* **3**, 21–32 (1997).

24. S. Razin, D. Yogev, Y. Naot, Molecular biology and pathogenicity of mycoplasmas., *Microbiol. Mol. Biol. Rev.* **62**, 1094–156 (1998).

25. M. a Meseguer *et al.*, Mycoplasma pneumoniae: a reduced-genome intracellular bacterial pathogen., *Infect. Genet. Evol.* **3**, 47–55 (2003).

26. H. Neimark, K. M. Kocan, The cell wall-less rickettsia Eperythrozoon wenyonii is a Mycoplasma., *FEMS Microbiol. Lett.* **156**, 287–91 (1997).

27. S. Lo, J. Shih, P. N. III, D. Wong, MM, Virus-like infectious agent (VLIA) is a novel pathogenic mycoplasma: Mycoplasma incognitus, *Am. J. Trop. Med. Hyg.* **41**, 586–600 (1989).

28. M. B. Rogers, Mycoplasma and cancer: in search of the link., *Oncotarget* (2011) (available at http://www.ncbi.nlm.nih.gov/pubmed/21508438).

29. S. Tsai, D. J. Wear, J. W. Shih, S. C. Lo, Mycoplasmas and oncogenesis: persistent infection and multistage malignant transformation., *Proc. Natl. Acad. Sci. U. S. A.* **92**, 10197–201 (1995).

30. D. Hanahan, R. a Weinberg, Hallmarks of cancer: the next generation., *Cell* **144**, 646–74 (2011).

31. M. Gerlic, J. Horowitz, S. Farkash, S. Horowitz, The inhibitory effect of Mycoplasma fermentans on tumour necrosis factor (TNF)-alpha-induced apoptosis resides in the membrane lipoproteins., *Cell. Microbiol.* **9**, 142–53 (2007).

32. D. Y. Logunov *et al.*, Mycoplasma infection suppresses p53, activates NF-kappaB and cooperates with oncogenic Ras in rodent fibroblast transformation., *Oncogene* **27**, 4521–31 (2008).

33. S. Zhang *et al.*, Mycoplasma fermentans infection promotes immortalization of human peripheral blood mononuclear cells in culture., *Blood* **104**, 4252–9 (2004).

34. C. M. Ketcham *et al.*, p37 Induces tumor invasiveness., *Mol. Cancer Ther.* **4**, 1031–8 (2005).

35. R. W. Parish, Invasive behavior of mouse sarcoma cells is inhibited by blocking a 37,000-dalton plasma membrane glycoprotein with Fab fragments, *Cell Biol.* **81**, 3747–3750 (1984).

36. C. Yang, G. Chalasani, Y.-H. Ng, P. D. Robbins, Exosomes released from Mycoplasma infected tumor cells activate inhibitory B cells., *PLoS One* **7**, e36138 (2012).

37. G. Paton, J. Jacobs, F. Perkins, Chromosome changes in human diploid-cell cultures infected with mycoplasma, *Nature* **207**, 43–45 (1965).

38. K. Namiki *et al.*, Persistent exposure to Mycoplasma induces malignant transformation of human prostate cells., *PLoS One* **4**, e6872 (2009).

39. M. Karin, T. Lawrence, V. Nizet, Innate immunity gone awry: linking microbial infections to chronic inflammation and cancer., *Cell* **124**, 823–35 (2006).

40. M. Karin, Nuclear factor-kappaB in cancer development and progression., *Nature* **441**, 431–6 (2006).

41. B. Zhang, J. Shih, D. Wear, S.-C. Lo, High-level expression of H-ras and c-myc oncogenes in mycoplasma-mediated malignant cell transformation, *Exp. Biol. Med.* **214**, 1535–3702 (1997).

42. S. Huang, J. Y. Li, J. Wu, L. Meng, C. C. Shou, Mycoplasma infections and different human carcinomas., *World J. Gastroenterol.* **7**, 266–9 (2001).

43. M. Pehlivan, S. Pehlivan, H. Onay, M. Koyuncuoglu, Z. Kirkali, Can mycoplasma-mediated oncogenesis be responsible for formation of conventional renal cell carcinoma?, *Urology* **65**, 411–4 (2005).

44. M. Kidder, P. J. Chan, I. M. Seraj, W. C. Patton, a King, Assessment of archived paraffin-embedded cervical condyloma tissues for mycoplasma-conserved DNA using sensitive PCR-ELISA., *Gynecol. Oncol.* **71**, 254–7 (1998).

45. P. J. Chan, I. M. Seraj, T. H. Kalugdan, a King, Prevalence of mycoplasma conserved DNA in malignant ovarian cancer detected using sensitive PCR-ELISA., *Gynecol. Oncol.* **63**, 258–60 (1996).

46. J. Pollard, Trophic macrophages in development and disease, *Nat. Rev. Immunol.* **9**, 259–270 (2009).

47. S. B. Coffelt *et al.*, Elusive identities and overlapping phenotypes of proangiogenic myeloid cells in tumors., *Am. J. Pathol.* **176**, 1564–76 (2010).

48. D. G. DeNardo, P. Andreu, L. M. Coussens, Interactions between lymphocytes and myeloid cells regulate pro- versus anti-tumor immunity., *Cancer Metastasis Rev.* **29**, 309–16 (2010).

49. M. Egeblad, E. Nakasone, Z. Werb, Tumors as organs: complex tissues that interface with the entire organism, *Dev. Cell* **18**, 884–901 (2010).

50. A. Sica, V. Bronte, Altered macrophage differentiation and immune dysfunction in tumor development, *J. Clin. Invest.* **117**, 1155–1166 (2007).

51. C. Murdoch, M. Muthana, C. E. Lewis, Hypoxia regulates macrophage functions in inflammation., *J. Immunol.* **175**, 6257–63 (2005).

52. B.-Z. Qian, J. W. Pollard, Macrophage diversity enhances tumor progression and metastasis., *Cell* **141**, 39–51 (2010).

53. A. Mantovani, A. Sica, Macrophages, innate immunity and cancer: balance, tolerance, and diversity., *Curr. Opin. Immunol.* **22**, 231–7 (2010).

54. M. Karin, F. R. Greten, NF-kappaB: linking inflammation and immunity to cancer development and progression., *Nat. Rev. Immunol.* **5**, 749–59 (2005).

55. L. C. Huysentruyt, P. Mukherjee, D. Banerjee, L. M. Shelton, T. N. Seyfried, Metastatic cancer cells with macrophage properties: evidence from a new murine tumor model., *Int. J. Cancer* **123**, 73–84 (2008).

56. L. M. Shelton *et al.*, A novel pre-clinical in vivo mouse model for malignant brain tumor growth and invasion., *J. Neurooncol.* (2010), doi:10.1007/s11060-010-0115-y.

57. M. K. Ranes *et al.*, N -butyldeoxynojirimycin reduces growth and ganglioside content of experimental mouse brain tumours., *Br. J. Cancer* **84**, 1107–14 (2001).

58. H. G. Crabtree, Observations on the carbohydrate metabolism of tumours., *Biochem. J.* **23**, 536–45 (1929).

59. C. E. Wenner, Pasteur and Crabtree effects--assay in cells., *Methods Enzymol.* **55**, 289–97 (1979).

60. M. Guppy, E. Greiner, K. Brand, The role of the Crabtree effect and an endogenous fuel in the energy metabolism of resting and proliferating thymocytes., *Eur. J. Biochem.* **212**, 95–9 (1993).

61. L. D. Marroquin, J. Hynes, J. a Dykens, J. D. Jamieson, Y. Will, Circumventing the Crabtree effect: replacing media glucose with galactose increases susceptibility of HepG2 cells to mitochondrial toxicants., *Toxicol. Sci.* **97**, 539–47 (2007).

62. C. Strelko *et al.*, Itaconic acid is a mammalian metabolite induced during macrophage activation, *J. Chem Soc.* **133**, 16386–16389 (2011).

63. A. Michelucci *et al.*, Immune-responsive gene 1 protein links metabolism to immunity by catalyzing itaconic acid production., *Proc. Natl. Acad. Sci. U. S. A.* **110**, 7820–5 (2013).

64. B. a McFadden, S. Purohit, Itaconate, an isocitrate lyase-directed inhibitor in Pseudomonas indigofera., *J. Bacteriol.* **131**, 136–44 (1977).

65. G. M. Tannahill *et al.*, Succinate is an inflammatory signal that induces IL-1β through HIF-1α., *Nature* **496**, 238–42 (2013).

66. J.-C. Rodríguez-Prados *et al.*, Substrate fate in activated macrophages: a comparison between innate, classic, and alternative activation., *J. Immunol.* **185**, 605–14 (2010).

67. D. S. Bredt, S. H. Snyder, Isolation of nitric oxide synthetase, a calmodulin-requiring enzyme., *Proc. Natl. Acad. Sci. U. S. A.* **87**, 682–5 (1990).

68. N. S. Forbes, A. L. Meadows, D. S. Clark, H. W. Blanch, Estradiol stimulates the biosynthetic pathways of breast cancer cells: detection by metabolic flux analysis., *Metab. Eng.* **8**, 639–52 (2006).

69. a Miccheli *et al.*, Metabolic profiling by 13C-NMR spectroscopy: [1,2-13C2]glucose reveals a heterogeneous metabolism in human leukemia T cells., *Biochimie* **88**, 437–48 (2006).

70. G. Yang, F. Coffman, E. Wheelock, Characterization and Purification of a macrophage-triggering factor produced in mycoplasma arginini-infected L5178Y cell cultures, *J. Immunol.* **94**, 2580–2591 (1994).

71. K. M. Boje, P. K. Arora, Microglial-produced nitric oxide and reactive nitrogen oxides mediate neuronal cell death., *Brain Res.* **587**, 250–6 (1992).

72. S. Marty, I. Dusart, M. Peschanski, GLIAL CHANGES FOLLOWING AN EXCITOTOXIC LESION IN THE CNS-I. MICROGLIA/MACROPHAGES, *Neuroscience* **45**, 529–539 (1991).

73. D. Laskin, K. Pendino, MACROPHAGES AND INFLAMMATORY MEDIATORS IN TISSUE INJURY, *Annu. Rev. Pharmacol. …* , 655–677 (1995).

74. A. Sakai, A. Kusumoto, Y. Kiso, E. Furuya, Itaconate reduces visceral fat by inhibiting fructose 2,6-bisphosphate synthesis in rat liver., *Nutrition* **20**, 997–1002 (2004).

75. G. Tevz, M. Bencina, M. Legisa, Enhancing itaconic acid production by Aspergillus terreus., *Appl. Microbiol. Biotechnol.* **87**, 1657–64 (2010).

76. M. a Selak *et al.*, Succinate links TCA cycle dysfunction to oncogenesis by inhibiting HIF-alpha prolyl hydroxylase., *Cancer Cell* **7**, 77–85 (2005).

77. P. Hochachka, T. Owen, J. Allen, GC, Multiple end products of anaerobiosis in diving vertebrates, *Physiol. Part B* **50**, 17–22 (1975).

78. T. Sanborn, W. Gavin, S. Berkowitz, T. Perille, M. Lesch, Augmented conversion of aspartate and glutamate to succinate during anoxia in rabbit heart, *Am. J. Physiol. Circ. Physiol.* **237**, H535 (1979).

79. E. Tomitsuka, K. Kita, H. Esumi, The NADH-fumarate reductase system, a novel mitochondrial energy metabolism, is a new target for anticancer therapy in tumor microenvironments., *Ann. N. Y. Acad. Sci.* **1201**, 44–9 (2010).

80. H. Takaku, M. Matsumoto, S. Misawa, K. Miyazaki, Anti-tumor Activity of arginine deiminase from mycoplasma arginini and its growth-inhibitory mechanism, *Cancer …* , 840–846 (1995).

81. D. S. Lind, Arginine and cancer., *J. Nutr.* **134**, 2837S–2841S; discussion 2853S (2004).

82. C. D. Mills, J. Shearer, R. Evans, M. D. Caldwell, Macrophage arginine metabolism and the inhibition or stimulation of cancer., *J. Immunol.* **149**, 2709–14 (1992).

83. F. Ribeiro-Dias, M. Russo, Mycoplasma arginini enhances cytotoxicity of thioglycollate-elicited murine macrophages toward YAC-1 tumor cells through production of NO, *J. Leukoc. …* (1999) (available at http://www.jleukbio.org/content/65/6/808.short).

84. L. Wojtczak, The Crabtree effect: a new look at the problem, *ACTA Biochim. Pol. Ed.* **43**, 361–368 (1996).

85. E. F. Greiner, M. Guppy, K. Brand, Glucose is essential for proliferation and the glycolytic enzyme induction that provokes a transition to glycolytic energy production., *J. Biol. Chem.* **269**, 31484–90 (1994).

86. M. T. Suchorolski, T. G. Paulson, C. a Sanchez, D. Hockenbery, B. J. Reid, Warburg and Crabtree Effects in Premalignant Barrett's Esophagus Cell Lines with Active Mitochondria., *PLoS One* **8**, e56884 (2013).

87. B. Chance, B. Hess, Spectroscopic Evidence Metabolic Control, *Science (80-.).* **129**, 700–708 (1959).

88. P. VanDemark, P. Smith, RESPIRATORY PATHWAYS IN THE MYCOPLASMA II. : Pathway of Electron Transport During Oxidation of Reduced Nicotinamide Adenine Dinucleotide by Mycoplasma Hominis, *J. Bacteriol.* **88**, 122–128 (1964).

89. P. J. Vandemark, P. F. Smith, Nature of Butyrate Oxidation By Mycoplasma Hominis., *J. Bacteriol.* **89**, 373–7 (1965).

90. R. Lynn, Oxidative metabolism of pleuropneumonia-like organisms, *Ann. N. Y. Acad. Sci.* **551**, 538–542 (1960).

91. T. Brenner, a Yamin, R. Gallily, Mycoplasma triggering of nitric oxide production by central nervous system glial cells and its inhibition by glucocorticoids., *Brain Res.* **641**, 51–6 (1994).

92. B. Beltrán, a Mathur, M. R. Duchen, J. D. Erusalimsky, S. Moncada, The effect of nitric oxide on cell respiration: A key to understanding its role in cell survival or death., *Proc. Natl. Acad. Sci. U. S. A.* **97**, 14602–7 (2000).

93. D. L. Granger, R. R. Taintor, J. L. Cook, J. B. Hibbs, Injury of neoplastic cells by murine macrophages leads to inhibition of mitochondrial respiration., *J. Clin. Invest.* **65**, 357–70 (1980).

94. L. Kastl *et al.*, TNF-α mediates mitochondrial uncoupling and enhances ROS-dependent cell migration via NF-κB activation in liver cells., *FEBS Lett.* **588**, 175–83 (2014).

95. P. Ranganathan, P. a Clark, J. S. Kuo, M. S. Salamat, R. F. Kalejta, Significant association of multiple human cytomegalovirus genomic Loci with glioblastoma multiforme samples., *J. Virol.* **86**, 854–64 (2012).

96. C. Soderberg-Naucler, A. Rahbar, G. Stragliotto, Survival in Patients with Glioblastoma Receiving Valganciclovir, *N. Engl. J. Med.* **369**, 985–6 (2013).

97. Y. Yu, A. J. Clippinger, J. C. Alwine, Viral effects on metabolism: changes in glucose and glutamine utilization during human cytomegalovirus infection., *Trends Microbiol.* , 1–8 (2011).

98. A. L. McCormick, V. L. Smith, D. Chow, E. S. Mocarski, Disruption of mitochondrial networks by the human cytomegalovirus UL37 gene product viral mitochondrion-localized inhibitor of apoptosis, *J. Virol.* **77**, 631 (2003).

99. J. Munger, S. U. Bajad, H. a Coller, T. Shenk, J. D. Rabinowitz, Dynamics of the cellular metabolome during human cytomegalovirus infection., *PLoS Pathog.* **2**, e132 (2006).

Introduction

Mycoplasmas of the Mollicutes class are considered the smallest self-replicating free-living prokaryotes (*1*). Mycoplasma 16S rRNA sequencing data used as a phylogenetic measure suggests that mycoplasmas originated from walled gram-positive eubacteria by degenerative evolution roughly 600 million years ago (*2*). Unlike their walled ancestors, the Mollicutes (soft skin) class lacks a cell wall and thus is resistant to common bacterial cell wall targeted antibiotics such as penicillin. Mycoplasmas range in size from 0.3μm to 0.8μm, which in turn reflects their small genome sizes. *M. genitalium* has the smallest genome (580 kb) of any organism that can be grown in pure culture and *M. hyorhinis* has the largest genome of the mycoplasmas (820 kb) (*3*) (*2*) (*4*). With limited coding capacity, the mycoplasma genus has stringent nutritional requirements for fatty acids, sterols, some amino acids, nucleic acids, and various vitamins/cofactors (*4*) (*5*). Dependence on metabolic precursors for life leads to the need of extremely complex media in order to cultivate and therefore study mycoplasmas. However, high mycoplasma infection rates show that mycoplasmas propagate well within or attached to mammalian cells in-vitro (*6*) (*1*).

Mycoplasma infection of cultured mammalian cells can falsify many metabolic and non-metabolic cellular assays including oxygen consumption assays (*7*), nitric oxide synthase activity (*8*), MTT viability assays (*9*), and mitochondrial protein synthesis determination (mycoplasma co-purified with the mitochondrial fraction) (*10*). In agreement, *M. hominis* infection of HeLa cells significantly altered genetic expression

profiles of 1972 genes (*11*). Another study found approximately 200 significant expression profile alterations in infected MCF7 cells and 70 of those genes were involved in metabolism (*12*). In Mycoplasma pneumoniae-infected individuals, tracheal cell explants were shown to have a decrease in ATP from respiration, possibly due to lower dehydrogenase activities of the cells (*10*). Similarly, M. hyorhinis is also capable of reducing the respiration system in heavily contaminated human skin fibroblast cells (*13*). Thus, mycoplasmas have a high potential for modulating host metabolism.

Regarding energy catabolism, mycoplasmas can be classified as fermentative or non-fermentative (*14*). Fermentative mycoplasmas are able to gain energy by substrate-level phosphorylation of ADP by glycolysis, specifically by the Embden-Meyerhof-Parnas (EMP) Pathway (*14*). Fermentation produces acid and occurs not to specifically make energy, but rather to oxidize NADH to allow glycolysis to continue to make energy (NAD+ is required for the 6th step of glycolysis) (*15*). Therefore, fermentative mycoplasmas are acidifiers and thus reducers of their environment. Some fermentative mycoplasmas such as *M. gallisepticum* have the ability to carry out a non-fermentative catabolism (*16*) (*17*) but viability and growth during a non-fermentative catabolism are unclear. However in the presence of glucose, fermentative mycoplasmas produce ***a net waste of acid***. In contrast, non-fermentative mycoplasmas do not produce a net waste of acid or alcohol, which indicates that their energy catabolism is mainly oxidative. In part, the oxidative catabolism of the non-fermentative mycoplasmas is perhaps due to the lack of